Remote Sensing of Environment 113 (2009) 2511–2526

Contents lists available at ScienceDirect

Remote Sensing of Environment

journal homepage: www.elsevier.com/locate/rse

A MODIS direct broadcast algorithm for mapping wildfire burned area in the western United States

S.P. Urbanski [a,*], J.M. Salmon [a,b], B.L. Nordgren [a], W.M. Hao [a]

[a] Missoula Fire Sciences Laboratory, Rocky Mountain Research Station, United States Forest Service, Missoula, Montana, USA
[b] Now with Land Cover and Surface Climate Group, Department of Geography and Environment, Boston University, Boston, Massachusetts, USA

ARTICLE INFO

Article history:
Received 4 May 2009
Received in revised form 15 July 2009
Accepted 18 July 2009

Keywords:
Fire
Burned area
Fire detection
MODIS

ABSTRACT

Improved wildland fire emission inventory methods are needed to support air quality forecasting and guide the development of air shed management strategies. Air quality forecasting requires dynamic fire emission estimates that are generated in a timely manner to support real-time operations. In the regulatory and planning realm, emission inventories are essential for quantitatively assessing the contribution of wildfire to air pollution. The development of wildland fire emission inventories depends on burned area as a critical input. This study presents a Moderate Resolution Imaging Spectroradiometer (MODIS) – direct broadcast (DB) burned area mapping algorithm designed to support air quality forecasting and emission inventory development. The algorithm combines active fire locations and single satellite scene burn scar detections to provide a rapid yet robust mapping of burned area. Using the U.S. Forest Service Fire Sciences Laboratory (FiSL) MODIS-DB receiving station in Missoula, Montana, the algorithm provided daily measurements of burned area for wildfire events in the western U.S. in 2006 and 2007. We evaluated the algorithm's fire detection rate and burned area mapping using fire perimeter data and burn scar information derived from high resolution satellite imagery. The FiSL MODIS-DB system detected 87% of all reference fires >4 km^2, and 93% of all reference fires >10 km^2. The burned area was highly correlated ($R^2 = 0.93$) with a high resolution imagery reference burn scar dataset, but exhibited a large over estimation of burned area (56%). The reference burn scar dataset was used to calibrate the algorithm response and quantify the uncertainty in the burned area measurement at the fire incident level. An objective, empirical error based approach was employed to quantify the uncertainty of our burned area measurement and provide a metric that is meaningful in context of remotely sensed burned area and emission inventories. The algorithm uncertainty is ±36% for fires 50 km^2 in size, improving to ±31% at a fire size of 100 km^2. Fires in this size range account for a substantial portion of burned area in the western U.S. (77% of burned area is due to fires >50 km^2, and 66% results from fires >100 km^2). The dominance of these large wildfires in burned area, duration, and emissions makes these events a significant concern of air quality forecasters and regulators. With daily coverage at 1-km^2 spatial resolution, and a quantified measurement uncertainty, the burned area mapping algorithm presented in this paper is well suited for the development of wildfire emission inventories. Furthermore, the algorithm's DB implementation enables time sensitive burned area mapping to support operational air quality forecasting.

Published by Elsevier Inc.

1. Introduction

Biomass fires emit large amounts of trace gases and particles (Ito & Penner, 2004; Michel et al., 2005; van der Werf et al., 2006; Wiedinmyer et al., 2006) and these emissions significantly influence the chemical composition of the atmosphere and the earth's climate system (Langmann et al., 2009; Lapina et al., 2006; Simpson et al., 2006). The pollutants released by biomass burning include greenhouse gases, photochemically reactive compounds, and fine and coarse particulate matter (PM). Biomass fire emissions comprise a substantial component of the total global source of carbon monoxide (40%), carbonaceous particulate matter (35%), and nitrogen oxides (20%) (Langmann et al., 2009). Fires influence climate both directly, by emitting greenhouse gases and aerosols, and indirectly, through secondary effects on atmospheric chemistry (e.g., ozone (O_3) formation) and aerosol and cloud microphysical properties and processes (Lohmann & Feichter, 2005; Naik et al., 2007). Biomass fire emissions contribute to air pollution by increasing the atmospheric levels of pollutants that are detrimental to human health and ecosystems, and degrade visibility. The air quality impacts occur through the emission of primary pollutants (e.g., PM) and the production of secondary pollutants (e.g., O_3,

* Corresponding author. Tel.: +1 406 329 4829.
E-mail address: surbanski@fs.fed.us (S.P. Urbanski).

0034-4257/$ – see front matter. Published by Elsevier Inc.
doi:10.1016/j.rse.2009.07.007

secondary organic aerosol) when organic compounds and nitrogen oxides released by fires undergo photochemical processing. Air quality can be degraded by transport and transformation of fire emissions on local (Muhle et al., 2007; Phuleria et al., 2005), regional (DeBell et al., 2004; Sapkota et al., 2005; Spracklen et al., 2007), and continental (Morris et al., 2006) scales.

In the United States, heightened concern over the detrimental health impacts of PM and O_3 have brought increased attention to fire emissions. Recently revised National Ambient Air Quality Standards (NAAQS) for $PM_{2.5}$ and O_3, the Regional Haze Rule (URL: http://www.epa.gov/visibility/program.html), and proposed rulemaking to regulate greenhouse gases have intensified the pressure on both air regulatory and land management agencies to address the air quality impact from biomass burning. Improved estimates of wildfire emissions are needed to support the forecasting and short-term management of regional air quality and to guide the development of land and air shed management policy. Both needs require accurate emission estimates with high temporal (hour to daily) and spatial resolution (sub-grid scale with respect to air quality models which have a minimum grid of about 4 km). Air quality forecasting and mitigation management have the additional requirement that emission estimates be generated in a timely manner to support real-time operations. In the regulatory and planning realm, wildfire emission inventories are needed to quantitatively assess the contribution of wildfire to air pollution. Reliable wildfire emission inventories are also needed for the development of strategies to improve or maintain air quality and to guide land management strategies (e.g. the use of prescribed fire to reduce the occurrence of catastrophic fire events).

The emission of a compound X from biomass burning during a given time period depends on burned area, vegetation loading and condition, fire behavior, and specific emission factors for X (Seiler and Crutzen, 1980). Burned area is one of the key uncertainties in estimating biomass burning emissions. Remote sensing from spaceborne platforms is a valuable method for fire detection and the measurement of burned area. High spatial resolution (30 m) Landsat TM and ETM+ imagery has been used to successfully measure burned areas and assess fire effects on vegetation and soil (Cocke et al., 2005; Epting et al., 2005; Key and Benson, 2006; Miller & Yool, 2002; van Wagtendonk et al., 2004). The high spatial and spectral resolution data provided by Landsat is well suited for mapping fire burned area and fire severity. However, with an observation interval of 16 days (Global Land Cover Facility, 2004 ; URL: http://glcf.umiacs.umd.edu/data/landsat/) the data lack the temporal resolution needed for air quality forecasting activities and the development of emission inventories.

Data from satellite sensors that provide higher temporal resolution with moderate to low spatial resolution (500 m to 4 km) such as the MODerate Resolution Imaging Spectroradiometer (MODIS), SPOT-VEGETATION, the Advanced Very High Resolution Radiometer (AVHRR), and the Geostationary Operational Environmental Satellite (GOES) have been widely used to characterize fire activity and estimate burned area (Pu et al., 2007; Simon et al., 2004; Tansey et al., 2004; van der Werf et al., 2006; Wiedinmyer et al., 2006; Zhang & Kondragunta, 2008). Daily burned area estimates covering the Contiguous United States (CONUS) have recently been developed using the GOES (Zhang & Kondragunta, 2008), MODIS (Wiedinmyer et al., 2006), and AVHRR sensors (Pu et al., 2007). Wiedinmyer et al. and Zhang and Kondragunta used active fire detections to estimate burned area, while Pu et al. developed their burned area product by combining active fire detections with changes in the surface reflectance.

The MODIS sensor on the polar orbiting Terra and Aqua satellites has been widely exploited for fire detection and estimation of burned area. The active fire product (MXD14, which refers to the active fire product derived from the MODIS instrument onboard either Terra or Aqua) is the most commonly used MODIS fire product, the details of which are provided by Giglio et al. (2003). While the MODIS active fire product has a nominal spatial resolution of 1-km, MODIS can detect fires as small as 100 m^2 under favorable conditions (Giglio et al., 2003). The common approach for estimating burned area from MODIS active fire detections assumes that the burned area is proportional to the fire pixel count. In some studies the burned area is assumed to be 1 km^2 per fire pixel count, scaled by fraction of vegetation cover (e.g. Wiedinmyer et al., 2006), while others have employed a proportionality constant that varies with vegetation cover and fire-pixel clustering (Giglio et al., 2006).

While MODIS active fire detections have been successfully aggregated to produce monthly burned area estimates on a coarse scale (1° spatial resolution) (Giglio et al., 2006), reliance on the MXD14 product alone to map daily burned area for air quality modeling and management is problematic. At mid-latitudes (at 45 °N) the timing of the Terra and Aqua MODIS overpasses results in a closely spaced (~90 min) midday pair and a nighttime pair with a six hour separation. This leads to omission errors for small, short-lived fires or fire activity ignited following the last pass of a pair. More importantly, the coarse temporal resolution may cause an underestimate of the burned area for large, rapidly moving fires which may traverse multiple MODIS pixels between overpasses. Recently implemented MODIS burned area products derived from changes in the daily surface reflectance time series address the limitations of the MXD14 product and provides a nominal spatial resolution of 500-m (Roy et al., 2008). Loboda et al. (2007) combined the MXD14 product with a differenced Normalized Burn Ratio (dNBR) time series derived from the MODIS Surface Reflectance 8-day composite (L3 Global 500 m product, Vermote et al., 2002) to map burned area in the western U.S. and Central Siberia.

The Missoula Fire Sciences Laboratory (FiSL) has a MODIS direct broadcast (DB) receiving station in place to demonstrate effective methods for monitoring biomass burning in near-real-time and predicting the impact of fire emissions on air quality. In this study we describe and evaluate a MODIS-DB burned area mapping algorithm designed to provide rapid-response burned area measurements for air quality forecasting and to support the development of emission inventories. The algorithm combines active fire locations (MXD14) and single scene burn scar detections (Li et al., 2004) for measurement of fire burned areas as part of a rapid-response wildland fire emissions system. The MODIS MXD14 algorithm is only capable of detecting fires active during the observation, and very recently burned areas that have retained significant heat. A burn scar algorithm enables the detection of burned area, providing information on fire activity that occurs between MODIS observations. Conceptually, the algorithm used in this study is similar to that developed by Fraser et al. (2000), who combined AVHRR active fire detections and normalized difference vegetation index, as well the method more recently employed by Loboda et al. (2007). As with Loboda et al. (2007), in our algorithm burn scar detection from the MODIS surface reflectance product is combined with the MODIS active fire product to map burned area. However, the algorithms differ substantially in their implementation. Our algorithm applies a series of spectral threshold tests to a single MODIS scene to identify burn scars, while Loboda et al. (2007) apply thresholds to the dNBR calculated from the 8-day composite containing the potential burn scar and the same composite period from one year prior.

The combination of active fire detection and a single scene burn scar detection algorithm is the key to producing a rapid, yet robust burned area measurement. The algorithm presented here was designed to provide daily observations of burned area for large (>4 km^2) wildfires in the western U.S., with a 1-km spatial resolution. This MODIS-DB burned area mapping algorithm was developed to produce emission estimates in support of operational air quality forecasting activities.

2. Data

2.1. MODIS active fire and burn scar detections

Direct broadcast MODIS data was collected via the receiving station operated by the Missoula Fire Sciences Laboratory (46.93 °N, 114.10 °W). The MODIS-DB dataset used for the burned area product in this study is unique to the location, configuration, and operation of the Missoula Fire Sciences Laboratory's receiving station. The MODIS-DB dataset includes data from both the Terra and Aqua satellites. However, because our MODIS-DB receiving station is single antenna (4.1 m), only one satellite broadcast may be received at a time. During periods when broadcasts from both Terra and Aqua could be received, the operation mode of the single antenna receiving station gave preference to overpasses affording the best coverage of the western U.S. The receiving station provided a Level-1B data set (geolocated, radiometrically calibrated) for each MODIS overpass received. The Level-1B data was processed using the standard MXD14 algorithm (Giglio et al., 2003) rendering the MODIS fire and thermal anomaly products. A single scene burn scar detection algorithm, described in Section 3.1, was applied to the Level-1B data to identify potentially burned pixels. With the exception of occasional hardware or software issues, the DB system was operated continuously during the study period (1 January 2006–31 December 2007). Our DB system experienced 18 days of downtime each year. Fire events in the reference datasets that were active primarily during our DB system's offline periods were excluded from the evaluation (Section 3.2). Ten fire events were excluded in 2006 and 27 fire events were excluded in 2007.

2.2. Incident data

Fire data collected by federal and state agencies was used to characterize recent fire occurrence (frequency, size, location, cover type), provide 'ground-truth' for our MODIS-DB burned area maps, and furnish records of total burned area for large geographic regions. For many large fire events, fire perimeter polygons are periodically mapped by incident management teams. These incident perimeter polygons are produced to support fire management activities, not map the area burned, and are therefore less than ideal as a reference dataset. Incident perimeters are deficient in meeting air quality emission inventory requirements in several ways: 1) perimeters are not produced on a regular basis or at a standard time, and they are not available for many fire events; 2) their purpose is identifying the fire perimeter, not mapping the area burned, and the area within a perimeter typically includes unburned regions, the average fraction of unburned to low severity burned area within incident fire perimeters was found to be 28% when compared to high resolution remote sensing observations (Schwind, 2008); 3) perimeters are measured using different methodologies (e.g. infrared or visual aerial survey, ground based global positioning system); 4) perimeters are not usually available in a timeframe that can support air quality forecasting activities and 5) perimeters are not collected at a central location in a timely manner. Incident perimeters typically provide a boundary that encompasses the true extent of burning. On occasion the incident management team may demobilize prior to the complete end of burning. In such a case, the 'final' incident perimeter may not completely encompass the area of fire activity. Further discussion regarding the use of incident perimeters as 'ground-truth' are provided by Key (2006).

For evaluation of our MODIS-DB burned area mapping algorithm, we obtained incident perimeters collected and maintained by the USGS Rocky Mountain Geographic Science Center (RMGSC) and made available through GeoMAC (URL: http://rmgsc.cr.usgs.gov/outgoing/GeoMAC/). 966 incident perimeters from 2006 and 2007 were used in this study. A subset of 370 large fire (>4 km^2) incident perimeter polygons were used as a reference dataset (hereafter referred to as the 'Incident Perimeter (IP) reference dataset') to calibrate and evaluate our MODIS-DB burned area mapping algorithm. The entire collection of 966 incident perimeters was used to evaluate the MODIS active fire detection algorithm applied to the data received by the FiSL DB station.

Point datasets containing daily information on fire location and size from Incident Management Situation Reports (IMSR or 'SIT reports') were obtained from the database maintained by National Interagency Fire Center (NIFC) in Boise, Idaho (National Fire and Aviation Management, 2008). Tabulations of annual burned area by state were acquired from the National Interagency Coordination Center (NICC, 2008). While the NICC dataset contains only summary statistics, it covers both wildfire and prescribed fire activity.

2.3. High resolution imagery products

Burned Area Reflectance Classification (BARC) maps for 142 fires in 2006 and 2007 were obtained from U. S. Forest Service, Remote Sensing Applications Center in Salt Lake City, Utah (URL: www.fs.fed.us/eng/rsac/baer , Clark & Bobbe, 2004). BARC maps are satellite-derived (usually Landsat TM) maps with pixels classified according to post-fire vegetation condition. Classification is based on the differenced Normalized Burn Ratio (dNBR), a sensitive method for identifying burned areas with high resolution imagery (Key, 2006; Key & Benson, 1999, 2006; Lentile et al., 2006). The four category BARC burn severity classifications are: unchanged/very low severity (class 1), low severity (class 2), moderate severity (class 3), and high severity (class 4). The classifications are based on dNBR thresholds chosen by an RSAC remote sensing analyst. Limited field validation of BARC maps gave these products an accuracy of 75% in identifying unburned areas (Bobbe et al., 2003). In this study, the BARC data is used to delineate unburned regions inside the incident perimeters (Section 2.2). All regions with BARC class >1 were classified as burned, providing a burn scar mask for each fire event. For the 2006 and 2007 BARC data used in this study, the typical threshold for BARC = 1 was dNBR<100. For a pixel with BARC = 1, 'unchanged or very low severity burn', the area after the fire was indistinguishable from pre-fire conditions.

BARC maps are a remote sensing product and do not provide an actual 'ground truth'. A few deficiencies of the BARC dataset must be emphasized here: 1) BARC maps are constructed at the request of Burned Area Emergency Rehabilitation Teams, they are not done for all fires, and the majority are forest fires; 2) BARC post-fire image acquisitions often occur before a fire is completely finished burning; 3) remote sensing methods often have limited detection for low intensity surface fires that occur under a closed, unaffected, or living canopy. Details and discussion of the BARC mapping and limitations of the imagery used in producing BARC maps are provided by Bobbe et al. (2003), Key (2006) and Safford et al. (2008).

2.4. Land cover–land use data

We used the University of Maryland modification of the International Geosphere-Biosphere Program (IGBP) land cover type classification scheme from the 1-km MODIS Level 3 Land Cover Product dataset (MOD12Q1 v4, URL: http://www-modis.bu.edu/landcover/userguidelc/index.html, Hansen et al., 2000) to characterize observed fire patterns by ecosystem type and evaluate land cover as a factor in the performance of our burned area algorithm. The Global Land Cover Characteristics (GLCC) dataset (Brown et al., 1999) USGS land cover/land use scheme was used in the burned area algorithm to filter out agricultural areas (Section 3). The fire detection and burned area products presented in this study were produced in 'real-time' from MODIS-DB data received by the FiSL station. During the study period, the burned area mapping algorithm employed the GLCC dataset. The

algorithm has since been changed to use the more recent and more widely used MOD12Q1. For our evaluation we chose to use MOD12Q1.

3. Method

3.1. MODIS-DB burned area algorithm

3.1.1. Active fire detection

The FiSL MODIS-DB receiving station provided a Level-1B data set for each MODIS overpass received (Section 2.1). The Level-1B data was processed using the standard MXD14 algorithm (Giglio et al., 2003) providing the MODIS active fire detections. The active fire detections were filtered using an agricultural mask derived from the GLCC (Section 2.4) to eliminate burning associated with agriculture.

3.1.2. Burn scar algorithm

The burn scar algorithm used in this study is a modified implementation of that described previously in Li et al. (2004). Here we briefly summarize the algorithm and describe our modifications. The method of burn scar detection is presented in Eqs. (1a)–(1e). This method consists of a series of threshold tests, culminating in a ratio of top of the atmosphere (TOA) apparent reflectance (ρ^*) in the 1.24 μm and 2.13 μm bands. In addition to the threshold tests of Eqs. (1a)–(1e), the land/water mask available in the MODIS Geolocation (MOD03) product is used to eliminate pixels containing water. In the final form of the algorithm, all pixels not filtered by the water mask and which satisfy the conditions Eqs. (1a)–(1e) are tentatively identified as burn scarred, pending contextual filtering.

$$0.05 < \rho^*_{1.24\mu m} < 0.2 \tag{1a}$$

$$\rho^*_{0.86\mu m} < 0.18 \tag{1b}$$

$$\rho^*_{2.13\mu m} > 0.05 \tag{1c}$$

$$0.10 < \rho^*_{1.64\mu m} < 1.0 \tag{1d}$$

$$0 \le \frac{\rho^*_{1.24\mu m} - 0.05}{\rho^*_{2.13\mu m}} < R_{th} \tag{1e}$$

In all equations ρ^*_λ represents the apparent reflectance (TOA) in the band of center wavelength λ. All of the bands utilized in the algorithm have a spatial resolution of 500 m. Eqs. (1a)–(1d) reduce false alarms associated with cloud shadows. The quantity R_{th} in Eq. (1e) controls the threshold which determines whether a pixel is considered burned. Li et al. (2004) recommends a threshold value between 0.8 and 1.0. Higher values of R_{th} result in more false alarms, while lower values reduce the algorithm's ability to penetrate smoke. We employed a threshold of $R_{th} = 0.8$, to minimize false detections. The thresholds in Eqs. (1a)–(1d) are the same as Li et al. (2004) with the exception of the 1.64 μm band lower threshold which was increased from 0.05 to 0.10 to minimize false detections.

Although the classification scheme effectively identifies burned pixels, operational use of the algorithm produced a large number of false detections. The false detection rate was reduced by implementing a contextual filter. Burn scar detections are eliminated if they are not proximate to a recent fire detection (based on the MXD14 algorithm). To be retained, burn scars must be within 5 km of any fire detection from the preceding 10 days. Pixels classified as burned by the Li et al. (2004) algorithm which do not satisfy this criterion are reclassified as unburned. The purpose of the algorithm is mapping wildfire burned area; therefore, burn scar detections are further filtered using an agricultural land mask (Section 2.4) to eliminate burning associated with agriculture.

The criterion balances the desire to restrict burn scar detections to recently burned areas against the need to consider detection limits related to smoke obstruction and rapid fire progression between observations. The daytime MODIS overpasses (which provide the surface reflectance observations) have a separation of ~90 min (at 45 °N), with last occurring in mid-afternoon. An active fire front may progress considerably in the 20+ hours between the mid-afternoon pass and the first pass of the next day, particularly in the late afternoon and early evening hours. The 5 km distance test allows for significant propagation of an active fire front between MODIS observations. Additionally, thick smoke may prevent burn scar detection for a period of time after the area is burned.

3.1.3. Fire event buffers and burned area

Active fire and single scene burn scar detections were combined to measure spatially resolved fire growth. The process by which fire and burn scar detections were transformed from a collection of dissociated points of regional scale to a set of "fire events" is illustrated in Fig. 1. While the collection of all fire events retains a regional scale, each individual fire event has a local extent. Fire events are produced exclusively from the MODIS-DB data, without reference to external reporting sources.

Fire event buffer generation is an iterative process. As shown in Fig. 1, "Current Fire Events", which are produced by the recent MODIS observation, are informed by previous runs of the fire event buffer generation algorithm on preceding MODIS observations ("Active Fire Events"). In the first step, "Growth and Seeding", current fire detections are added to existing fire events if they are within 5 km of an event. Fire detections which cannot be associated with an existing fire event are considered new, and a new "event" is created. The second step, "Growth by Proximity", adds burn scar detections (which have been filtered by

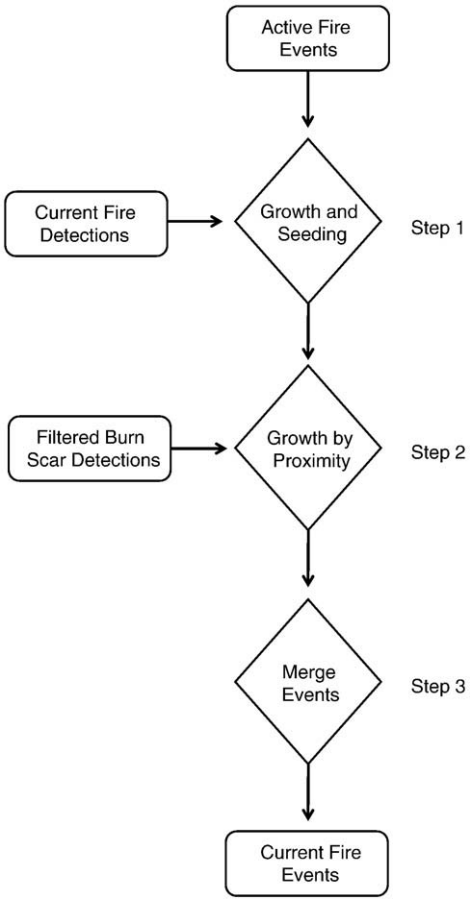

Fig. 1. Process to aggregate active fire and burn scar detections into fire events.

the process described in Section 3.1.2) to the nearest fire event that is within 5 km. Burn scar detections that are not within 5 km of a fire event are flagged as false detections and do not contribute to fire event buffer generation and burned area mapping. New fire events are never produced by a burn scar detection.

After fire events have accumulated new detections, a new fire event buffer is constructed by the process of "buffering". Each detection is buffered with a circle of an appropriate diameter (500 m for burn scars, 1 km for active fire detections) about its center point. Using the new fire event buffer, the final step is to check whether two or more fire events have physically merged or have become close enough to be treated as a single event. When two fire events that are not in physical contact are 'merged', no additionally burned area is created. Rather the two separate polygons are combined into a single multi-part polygon. Fire events are considered to have merged into a single fire event if their fire event buffers are less than 5 km apart at the point of nearest approach. These fire event buffers grow with the addition of detections, merge together when appropriate, and become 'inactive' after 10 days without any active fire detections.

A daily burned area grid product was created by projecting the fire event buffers onto a 1-km × 1-km CONUS grid. The selection criterion for identifying burned grid cells was to select cells whose center point fell within any of the fire event buffers. With each MODIS overpass received, the updated fire event buffers were placed on the 1-km CONUS grid. At 12 GMT (06 MDT) the burned area grid for all of the MODIS overpasses processed in the preceding 24 h are compared against a cumulative burned area grid which tracks the cumulative burned area for 90 days. Comparison against the cumulative burned area grid identifies the areas newly burned in the preceding 24 h, providing the burned area growth for that day. The MODIS-DB burned area grid product for 2006 and 2007 is available at URL: < http://www.smoke-fire.us/misc/modba >.

3.2. Evaluation

3.2.1. Fire detection

Performance of our MODIS-DB burned area algorithm in detecting fire occurrence was validated using the final incident perimeters of 966 fire events from 2006 and 2007 (Section 2.2). The MODIS-DB detection rate was evaluated according to fire size and land cover, using the University of Maryland modification of the International Geosphere-Biosphere Program (IGBP) land cover type classification scheme (Hansen et al., 2000) of the MODIS Level 3 Land Cover Product (Section 2.4). A fire event was considered detected if the incident fire perimeter polygon was within 1 km of any MODIS-DB fire event buffer. Evaluation of the fire detection rate by land cover type used the UMD cover type scheme aggregated to 6 cover types (forest, savanna, shrub, grassland, crop, and barren). The MODIS Land Cover Product was converted to polygons and intersected with the incident polygons. The dominant cover type by area for each fire event was taken as that event's cover type for the analysis.

3.2.2. Burned area measurement

The ability of our MODIS-DB algorithm to measure fire burned area was evaluated using two 'ground truth' datasets: the IP reference dataset (Section 2.2) and the BARC reference dataset (Section 2.3). With the exception of select fire events that have been studied with comprehensive post-fire ground measurements, there is no genuine 'ground truth' for evaluating remote sensing burned area products. A primary goal of our study was to quantify the uncertainty of our MODIS-DB burned area product at the fire event level. Achieving this goal requires a large number of reference fire events. The need for a large reference dataset leaves us with essentially two options for reference datasets which serve as a proxy for 'ground truth'. These are incident perimeters and remote sensing imagery. We chose to combine incident perimeters (from our IP reference dataset) with remote sensing to produce our primary reference dataset, our "BARC reference dataset".

For the reasons discussed in Section 2.2, and reemphasized below, incident perimeters generally provide a boundary for the true extent of burning. As a boundary for the true extent of burning, incident perimeters typically encompass areas not burned and thus in general are an overestimate of the true burned area. We have attempted to correct for the unburned areas within the incident perimeters using remotely sensed imagery — the BARC data. By using the BARC data to delineate unburned areas within the incident perimeters, we have assembled a reference dataset (our "BARC reference dataset") that we believe is well suited for our purposes. The number of observations and breadth of coverage (fire size and cover type) of the BARC reference dataset has allowed us to characterize the uncertainty of our MODIS-DB burned area product in the western U.S. (Section 4.3). We also evaluated our MODIS-DB burned area product against the incident perimeter data alone (our "IP reference dataset") and have included these results. Often times, when high resolution remote sensing data are used as a reference dataset for assessing moderate resolution remote sensing burned area methods, the presentation implies the high resolution data is a 'genuine ground truth'. All remote sensed burned area products have substantial potential for error. We believe including both evaluations illustrates the uncertainty in 'true' burned area.

The BARC reference dataset was assembled by combining the burn scar masks derived from BARC images (Section 2.3) and final incident fire polygons from the IP reference dataset (Section 2.2) for 142 events. Final incident fire polygons were used to extract the fire perimeter area from each BARC image. Next, regions within the fire perimeter indicated as unburned by the BARC burn scar mask were removed, providing the final burned area polygons, i.e. the BARC reference dataset. As discussed above and in Section 2.2, a sizeable fraction of the area inside incident perimeters is typically unburned or only lightly burned. In the BARC dataset used for validation, 31% (±15%) ($\mu \pm 1\sigma$) of the incident perimeter area had dNBR values deemed consistent with an unburned to very low burn severity surface. This fraction is in agreement with the 28% 'unburned to low burn severity' reported in the comprehensive Monitoring Trends in Burn Severity (MTBS) study (Schwind, 2008), which examined over 100,000 km^2 of burned area from 3050 fires which occurred in the western U.S. between 1984 and 2005. The collection of MODIS-DB burned area grid cells compared against each large fire polygon (from the IP or BARC reference dataset) were selected by visual inspection. MODIS-DB burned area grid cells that predated the reported incident start date by more than two days were excluded from the comparison. The incident start date was obtained from the NIFC IMSR database.

4. Results

4.1. MODIS-DB burned area algorithm

Examples of the algorithm applied to reference fires is provided in Figs. 2–4. The Chippy Creek Fire (Fig. 2) and Shower Bath Complex Fire (Fig. 3) occurred in Douglas-fir/lodgepole pine forests in the Northern Rocky Mountains in the summer of 2007. The Black Pine 2 Fire (Fig. 4) burned sagebrush shrublands and grasslands in the Eastern Great Basin (SE Idaho). Figs. 2–4 show buffered active fire and burn scar detections, and the resultant fire event buffers and burned area grid product overlaid on the BARC reference dataset. For the Chippy Creek Fire, the MODIS-DB gridded burned area (Fig. 2d) is 396 km^2 vs. 276 km^2 for the validation burn scar, a ratio (0.70) comparable to the mean bias determined for the entire dataset (0.64, Section 4.3). Interestingly, the burned area based on the buffered MODIS-DB burn scar detections alone (285 km^2) roughly equals the validation burned area with some help from offsetting errors of omission and

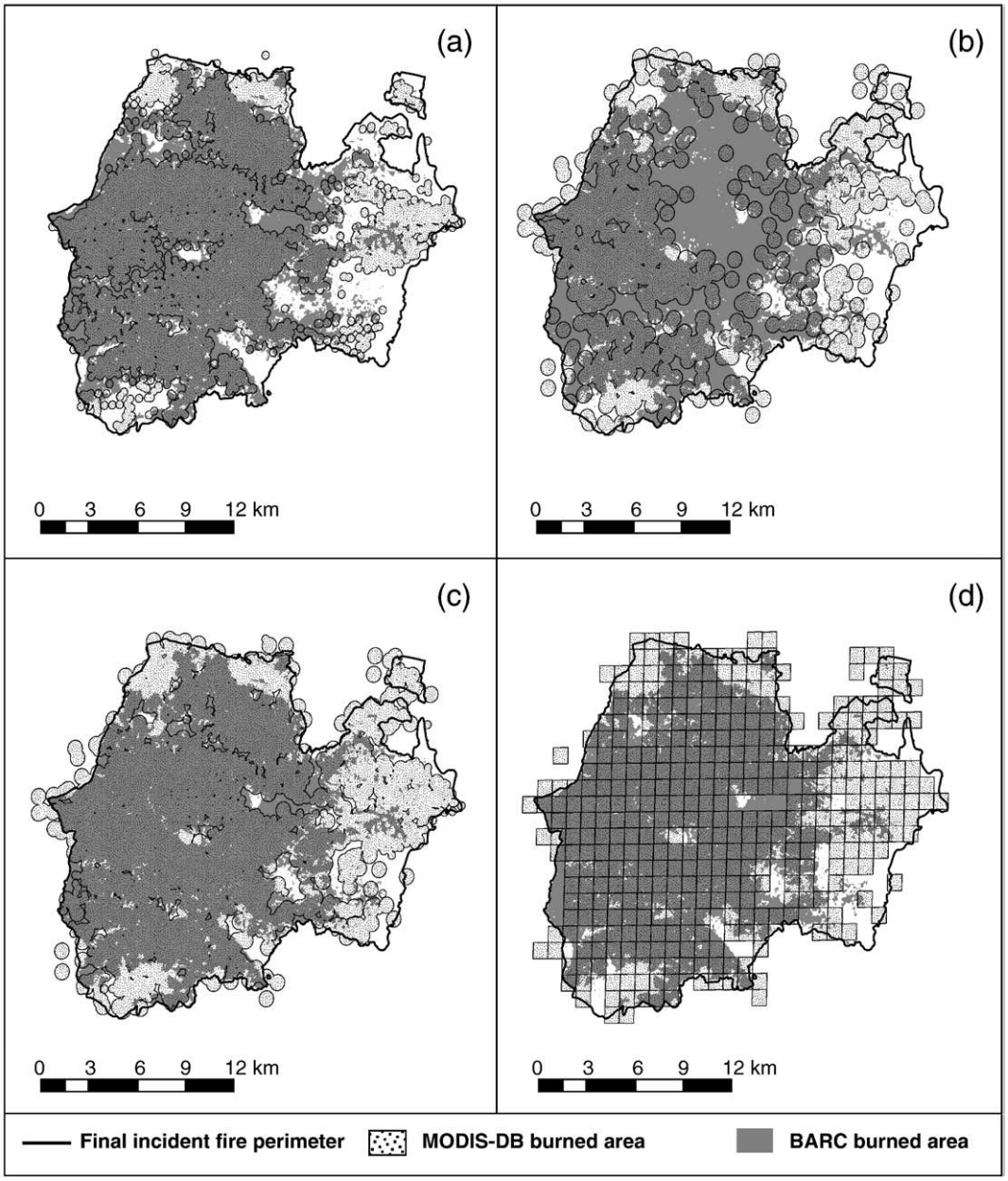

Fig. 2. MODIS-DB fire products overlaid on the high resolution validation dataset for the Chippy Creek Fire (July 31–September 9, 2007, 47.81 °N, 115.00 °W, Sanders County, Montana): a) buffered burn detections; b) buffered active fire detections; c) fire perimeter from combined burn scars and buffered active fire detections; d) burned area grid product.

commission. The Shower Bath Complex (Fig. 3) is one of the more dramatic cases of the algorithm overestimating the burned area and exemplifies a weakness in the algorithm. The burned area grid product (611 km^2) for this fire event is more than double the burned area of the BARC validation burn scar (286 km^2), largely as a result of false burn scar detections on the periphery of the fire perimeter. For the case of the Black Pine 2 Fire, the burned area grid product closely matches the reference data in both total burned area (MODIS-DB = 284 km^2 vs. 259 km^2 BARC data) and spatial distribution (Fig. 4).

4.2. Detection–evaluation

The performance of the FiSL MODIS-DB burned area algorithm in detecting fire occurrence was validated using the IP reference dataset of 966 fires from 2006 and 2007 (Section 3.2.1). Our algorithm requires a MODIS active fire detection, based on the MXD14 algorithm, to initiate a fire event (Section 3.1.3). Therefore, the fire detection rate of our algorithm is, in fact, the MODIS active fire detection rate for the FiSL DB system. The detection rate is presented in Fig. 5, categorized by fire size and land cover type. The 'total' category in Fig. 5 includes the results for 55 savanna fires which were not plotted separately. All but 7 of the fires classified as savanna fires were located in California. The overall detection rate is 87% for fires larger than 4 km^2 and 93% for fires larger than 10 km^2. The detection rate was 100%, 75%, and 70% for conifer forest, grassland, and shrubland fires exceeding 2 km^2. Regardless of fire size, the MODIS-DB active fire detection algorithm is most effective at detecting forest fires.

4.3. Burned area–evaluation

The performance of our algorithm was evaluated assuming a linear relationship with between the MODIS-DB burned area measurement and the 'true' burned area (Section 3.2.2):

$$A = a0 + a1 \times MOD \quad (2)$$

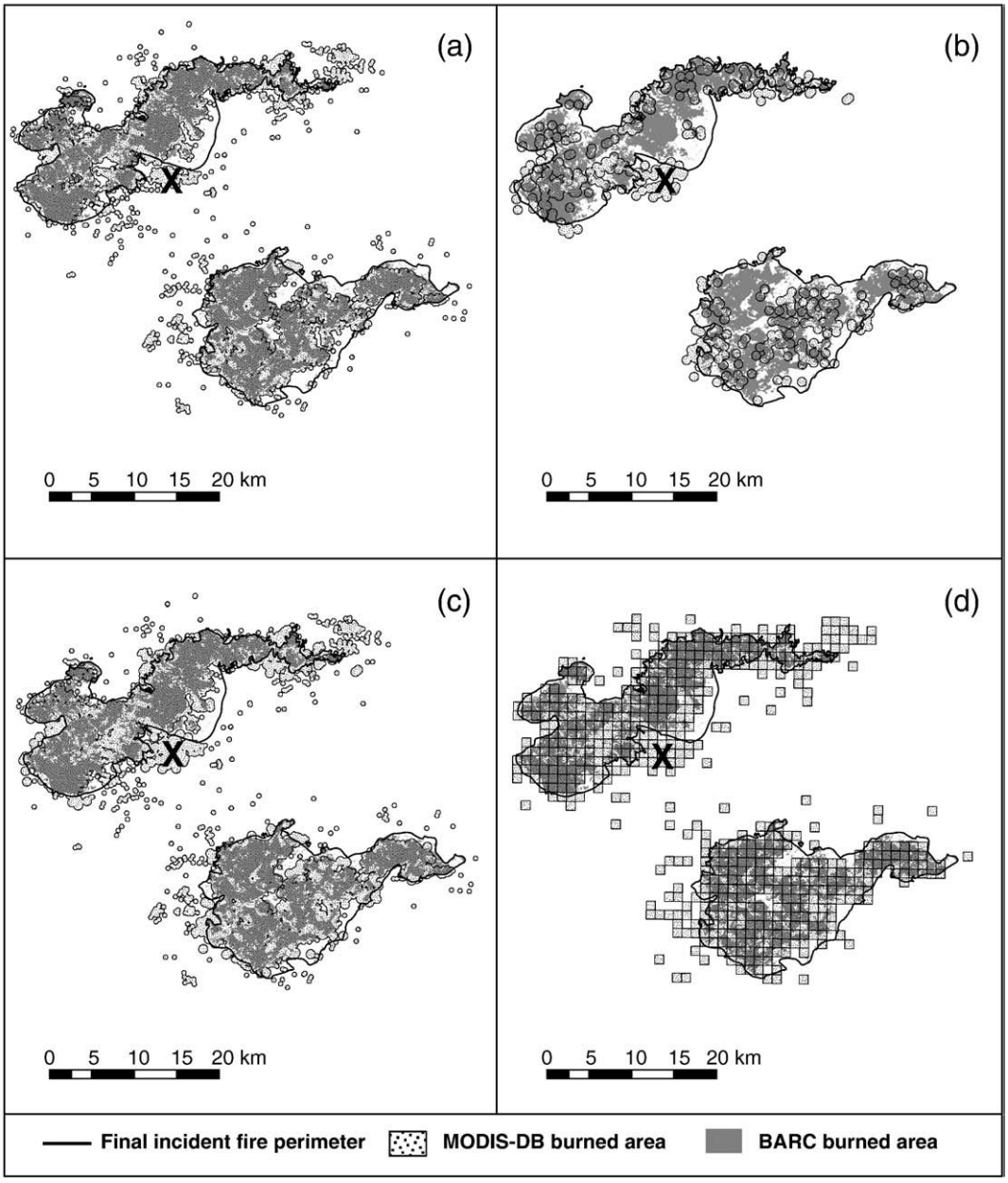

Fig. 3. MODIS-DB fire products overlaid on the high resolution validation dataset for the Shower Bath Complex Fire (July 15–September 30, 2007, 44.73 °N, 114.68 °W, Lemhi County, Idaho): a) buffered burn detections; b) buffered active fire detections; c) fire perimeter from combined burn scars and buffered active fire detections; d) burned area grid product. The 'X' marks a feature of interest discussed in Section 5.2.1.

where A is the 'true' fire event burned area, MOD is the MODIS-DB gridded burned area (3.1.3) associated with each fire event A, and a0 and a1 are regression coefficients. Eq. (2) provides the calibration for our MODIS-DB burned area measurement. We evaluated Eq. (2) using each reference burned area dataset (IP, Section 2.2 and BARC, 2.3, 4.1) as a surrogate for A, the 'true' burned area. The MODIS-DB burned area is plotted versus the BARC reference burned area in Fig. 6a, with a close-up of the lower size range provided in Fig. 6b. Fig. 6a and b includes a median linear regression best-fit line to Eq. (2), as well the 90% prediction interval (see below). In an effort to ensure our analysis was not unduly influenced by outliers, we evaluated Eq. (2) using both median regression (MR) and ordinary least-squares (OLS) regression. Median regression (quantile regression with $q = 0.50$) is generally less sensitive than OLS to outliers and extreme data points (Koenker, 2005; Wilcox, 2005). Comparison of the fire event burned areas from the MODIS-DB and IP reference datasets is shown in Fig. 7. The calibration results associated with Figs. 6 and 7 are listed in Table 1. The optimized coefficients (Table 1) were determined by combining median regression with a bootstrap sampling approach (Efron & Tibshirani, 1993). Two important features of Figs. 6 and 7 should be noted. The scatter about the MR best-fit line increases with fire size and there is an apparent regime change in the data around a fire size of 40 km^2. This variability of the errors across observations, called heteroscedasticity, violates a key assumption of OLS analysis — constant variance in the error term. The impact of this feature is discussed below. An important characteristic of the dataset not obvious from Figs. 6 and 7, is that the residuals of the fit to Eq. (2) are not normally distributed.

The IP reference dataset is comprised of polygons that identify the boundary of the area impacted by fire, and thus, this dataset provides an upper limit for the 'true' burned area. Using BARC maps to identify unburned regions within the incident perimeters should provide a more accurate representation of the 'true' burned area (see Sections 2.2 and 2.3). We have therefore, chosen the BARC reference dataset as

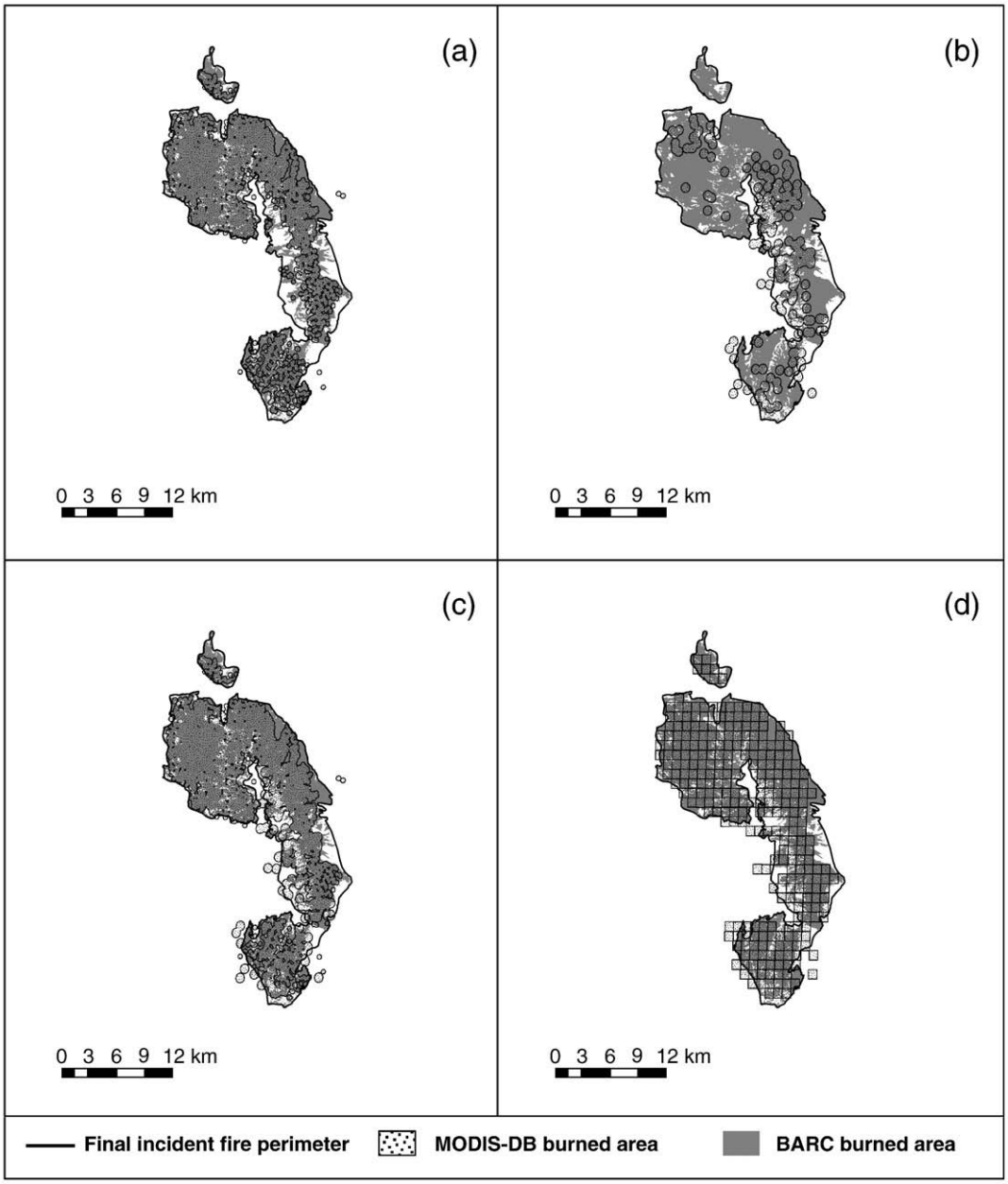

Fig. 4. MODIS-DB fire products overlaid on the high resolution validation dataset for the Black Pine 2 Fire (July 6–September 6, 2007, 42.18 °N, 1135.24 °W, Cassia County, Idaho): a) buffered burn scar detections; b) buffered active fire detections; c) fire perimeter from combined burn scars and buffered active fire detections; d) burned area grid product.

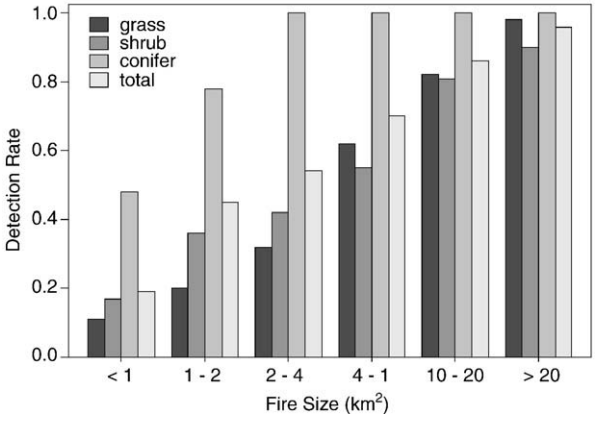

Fig. 5. FiSL MODIS-DB fire detection rate for 966 wildfires in the western U.S. during 2006 and 2007.

the 'ground truth' burned area for calibration and evaluation of our MODIS-DB algorithm. However, we urge readers to remain cognizant of the BARC dataset's limitations (Section 2.3) throughout the ensuing discussion.

The purpose of the MODIS-DB burned area mapping algorithm is to provide burned area estimates, at the fire event level, for the development of wildfire emission inventories. The emission inventories will be used to forecast and evaluate the impact of wildfires on regional air quality. Therefore, it is critical to provide uncertainty estimates for our MODIS-DB burned area measurement. Uncertainty is typically expressed as an interval about a measurement result that is expected to encompass a specified probability range of the true value. When the probability distribution characterized by a measurement result y and its combined (random and systematic) standard uncertainty u_c are approximately normal, the interval $y \pm u_c$ is expected to encompass about 68% of the measurand values, and u_c is commonly reported as the uncertainty ('1σ uncertainty'). In our

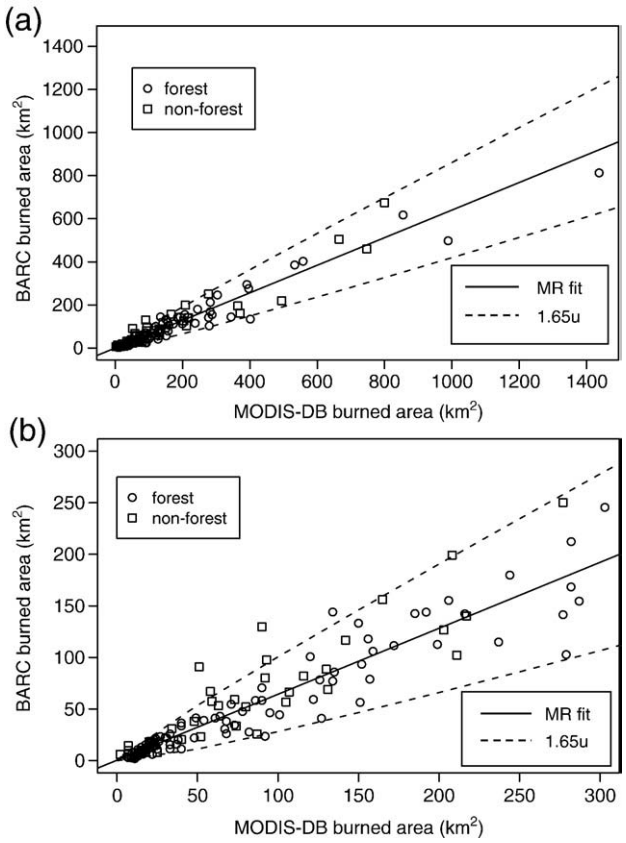

Fig. 6. Calibration of MODIS-DB burned area grid product against the BARC reference burned area for 142 fires events. MR = median regression best-fit line (Section 4.3), 1.65*u* is the approximate 90% prediction interval based on the empirical error function (Section 4.3, Fig. 8): a) all reference fires; b) close-up for reference fires less than 200 km^2.

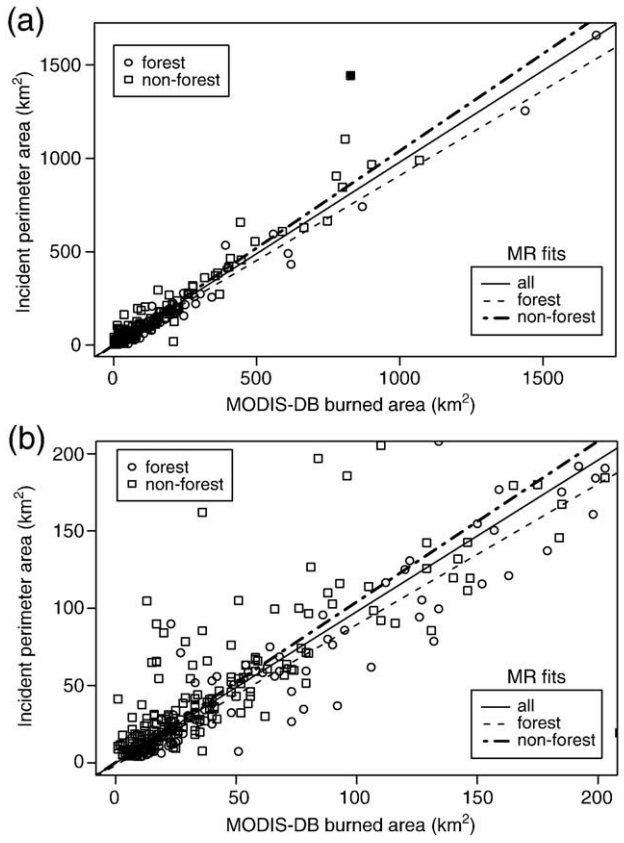

Fig. 7. MODIS-DB burned area grid product plotted against the incident perimeter area. All lines are median regression best-fit lines. The data point denoted with the filled square marker was excluded from the analysis. a) all reference fires; b) close-up for reference fires less than 200 km^2.

study, the burned area data are not normally distributed and the variance of the calibration residuals increases with fire event size; therefore, applying standard approaches may result in inaccurate uncertainty estimates. We have chosen to define uncertainty as the error cone we expect to envelop approximately 68% of fire event burned area values of which the calibrated MODIS-DB burned area measurement (Eq. (2)) is an estimate. We have chosen an empirical error estimation approach to identify this error cone and thereby quantify the uncertainty of our MODIS-DB burned area measurement as a function of fire size.

We explored several functional forms before choosing a power function. In Eq. (3a), below, u is the uncertainty in the MODIS-DB gridded burned area measurement, MOD. The coefficients in Eq. (3a) were evaluated as follows: 1) the MODIS-DB burned area (MOD) and residuals from the calibration vs. the BARC reference dataset (Eq. (2), Table 1) were assigned to 14 size bins, 2) we calculated the RMSE of Eq. (2) ($RMSE_{bin}$) and the mean MODIS-DB burned area (MOD_{bin}) for each size bin, 3) we substituted $RMSE_{bin}$ and MOD_{bin} into Eq. (3a), and regressed $RMSE_{bin}$ against MOD_{bin}, optimizing the power function relationship of the substituted equation (Eq. (3b)). For the reasons discussed above, our uncertainty analysis was limited to evaluation against the BARC reference dataset.

$$u = b0 + b1 \times (MOD)^{b2} \tag{3a}$$

$$RMSE_{bin} = b0 + b1 \times (MOD_{bin})^{b2} \tag{3b}$$

A non-linear least squares procedure (tangent-linear, Bates & Chambers, 1992) was used to derive optimized values for parameters b0, b1, and b2 (Fig. 8). The optimized equation is excellent in describing the variability of $RMSE_{bin}$ (Fig. 8). The fit statistics (R^2, RMSE), coverage of calibration residuals, and the estimated uncertainty changed little when the number of size bins used in the analysis was varied from 10 to 15.

The purpose of this exercise is to construct an objective process which is qualitatively similar to our definition of measurement uncertainty. We believe the RMSE predicted with Eq. (3a), using the optimized parameters in Fig. 8, provides a meaningful measure of the uncertainty in our MODIS-DB gridded burned area across the span of fire sizes used for calibration in this study. The empirical uncertainty cone derived via this approach satisfies our uncertainty definition. Seventy seven percent of the BARC reference burned area values fall within the uncertainty bounds (inset Fig. 8). When a coverage factor of 1.65 is applied to our empirical uncertainty, 92% of the BARC reference burned area values are enveloped by the resulting uncertainty bounds, thus providing the 90% prediction interval for our calibrated MODIS-DB burned area measurement. As intended, the coverage provided by our empirically derived uncertainty is comparable to that of a standard uncertainty for normally distributed data (i.e. coverage of ~68% for 1σ, and 90% for 1.65σ). In addition to providing the intended coverage, the empirical uncertainty cone captures the variability of the measurement error across the observations (Fig. 8 inset). The calibrated burned area, measurement uncertainty, and percent uncertainty are provided in Table 2 for a range of MODIS observed burned areas.

Many satellite based burned area mapping methods apply cover type or ecosystem type dependent thresholds for identifying burn scars (e.g. Loboda et al., 2007; van der Werf et al., 2006). We expected the effectiveness of our burn scar algorithm to vary with cover type and tested for such an effect. A common test for statistical significance

Table 1
Optimized parameters and fitting statistics for calibration of the MODIS-DB burned area against the reference dataset (Eq. (2)).

Evaluation[a,f,g]	a0[b]	a1[c]	R^2	RSE[d]	MA%E[e]
Calibration vs. BARC reference dataset					
Forest and non-forest $n=142$					
MR[h]	0.23 ± 2.04	0.64 ± 0.05	0.93	411.8	35.0
OLS[h]	3.11 ± 4.08	0.62 ± 0.04	0.93	408.9	43.2
Forest $n=94$					
MR[h]	-1.06 ± 2.11	0.63 ± 0.06	0.95	295.3	31.9
OLS[h]	2.14 ± 3.68	0.60 ± 0.01	0.95	286.3	43.1
Non-forest $n=48$					
MR[h]	2.78 ± 3.07	0.67 ± 0.09	0.92	271.4	35.0
OLS[h]	2.93 ± 7.05	0.68 ± 0.03	0.92	265.8	32.7
Calibration vs. IP reference dataset					
Forest and non-forest $n=371$					
MR[h]	-0.19 ± 0.86	0.98 ± 0.04	0.96	749.0	35.9
OLS[h]	3.02 ± 2.15	0.98 ± 0.03	0.96	746.6	44.6
Forest $n=122$					
MR[h]	-1.63 ± 1.22	0.91 ± 0.05	0.98	367.7	30.6
OLS[h]	-1.42 ± 3.16	0.92 ± 0.04	0.98	365.8	31.3
Non-forest $n=247$					
MR[h]	0.13 ± 0.70	1.04 ± 0.03	0.95	594.5	36.0
OLS[h]	-3.16 ± 2.60	1.05 ± 0.04	0.95	591.9	44.0

[a] Evaluation of equation Eq. (2) OLS: ordinary least squares regression, MR: median regression.
[b] a0: intercept with standard error.
[c] a1: slope with standard error.
[d] RSE: root square error.
[e] MA%E: mean absolute percent error.
[f] The Breusch–Pagan test for homogeneity (H_0: variance of the regression residuals are homogeneous) was applied to each regression with the result that H_0 was rejected at $p<0.001$ for each case.
[g] The Shaprio–Wilk normality test (H_0: residuals are normally distributed) was applied to each regression with the result that H_0 was rejected at $p<0.001$ for each case.
[h] No attempt has been made to adjust the MR and OLS parameter errors for heteroscedasticity, therefore error bounds for the regression parameters (a0 and a1) may not provide sufficient probability coverage.

Table 2
Estimated uncertainty of the calibrated MODIS-DB burned area measurement.

Burned area		Burned area uncertainty	
MODIS-DB gridded burned area measurement[a]	Calibrated MODIS-DB gridded burned area measurement[b]	Uncertainty[c] (km^2)	Percent[d]
10	6.6	±3.8	±58
25	16.2	±7.6	±47
50	32.2	±12.8	±40
100	64.2	±22.0	±34
200	128.2	±37.8	±29
400	256.2	±65.1	±25
800	512.2	±112.3	±22

Based on calibration vs. BARC reference dataset. Uncertainties from Eq. (3a). All values are in units of km^2 except the percent uncertainty.
[a] Fire event MODIS-DB burned area measurement (MOD in Eq. (2)).
[b] Calibrated MODIS-DB burned area as predicted by Eq. (2) using MR parameters from calibration versus BARC reference dataset in Table 1.
[c] Uncertainties are ±RMSE predicted by Eq. (3a) using optimized parameters given in Fig. 8 (b0 = 0.31, b1 = 0.57, b2 = 0.79).
[d] Percent uncertainty given as percent of calibrated MODIS-DB burned area measurement.

of a group effect (in this case cover type) is Chow's test for equality among regression coefficients (Chow, 1960; Glantz, 2002). However, our data set is not normally distributed and does not have constant variance of errors across the observations, and thus fails to satisfy the assumptions of the Chow test statistic. Concerns regarding validity of the Chow test for our dataset were addressed by using a multi-response permutation procedures (MRPP) analysis. The MRPP analysis does not assume variance homogeneity and should provide a reasonable analysis for data with heterogeneous variance and/or non-normality (Mielke & Berry, 2001; Turner, 2006). The residuals of Eq. (2) were tested for similarity among two cover groups (forest and non-forest) using MRPP analysis (Mielke & Berry, 2001; Turner, 2006). Our analysis indicated no cover type effect ($p=0.07$) for the calibration based on the BARC reference dataset (Fig. 6). In any case, the difference in the calibration slopes between forest and non-forest cover types is minor (~5% for MR fits, Table 1), as is the ~4 km^2 difference in intercepts when the dominance of large fire events is considered (see Appendix A). However, the calibration derived using the larger IP reference dataset (Fig. 7) did exhibit a cover type effect ($p<0.001$). This influence of cover type may reflect the difference in the burned fraction of the perimeter area observed between forested and non-forested areas. In the BARC reference dataset, which is a 142 member subset of the 370 member IP dataset, the unburned fraction ($\mu\pm\sigma$) was 0.65 ± 0.15 and 0.75 ± 0.15 for forest and non-forest cover types, respectively. The ratio of unburned fractions (0.65/0.75) equals the ratio of the calibration slopes obtained when the cover types are treated separately (0.91/1.04, Fig. 7, Table 1). This suggests the cover type effect indicated by the IP reference dataset may result in part from the difference in the fraction of interior perimeter area that is burned, and does not exclusively stem from a cover type dependent response of the MODIS-DB burned area mapping algorithm.

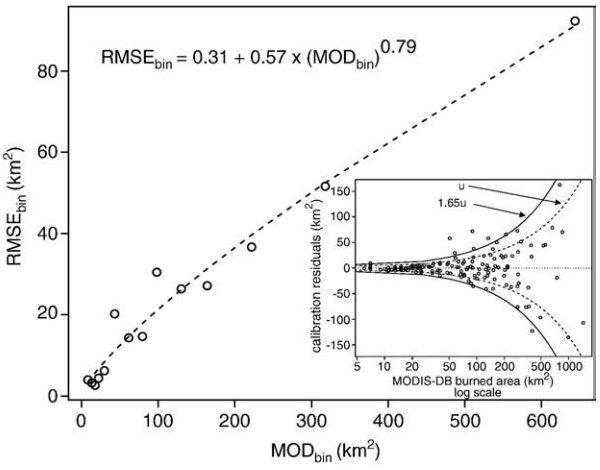

Fig. 8. Empirical error function for MODIS-DB burned area algorithm calibration curve (Section 4.3). The *x*-axis is the average MODIS-DB measured burned area for each of 14 size bins (MOD_{bin}) and the *y*-axis is the RMSE of the algorithm burned area calibration curve (Eq. (2)) for each size bin ($RMSE_{bin}$). The open circles are MOD_{bin} versus $RMSE_{bin}$. The dashed line is the RMSE predicted by the optimized empirical error function (Eq (3)). The inset figure plots residuals of the calibration (Eq. (2), Table 1) against the MODIS-DB burned area (open circles). The *x*-axis is log scale. The dashed (solid) curve is ±1 RMSE (±1.65 RMSE) as estimated with the empirical error function and envelopes 77% (92%) of the residuals.

4.4. Burned area

The annual burned area estimated by the FiSL MODIS-DB algorithm in 2006 and 2007 is displayed in Fig. 9. The 1-km burned area grid product (Section 3.1.3) was aggregated to 22-km×22-km grid cells to provide a better visualization of the magnitude and spatial distribution of the burned area. Monthly large fire (>4 km^2) burned area by state, with estimated uncertainties, is presented in Fig. 10.

Statewide monthly burned areas and burned area uncertainty estimates were calculated by applying the calibration (Table 1) and the empirical uncertainty function (Fig. 8) to each distinct fire event using Eqs. (4) and (5). The identification and growth of fire events is described in Section 3.1.3. In Eqs. (4) and (5), MOD_i is the MODIS-DB measured burned area growth for each distinct fire event and nf is the

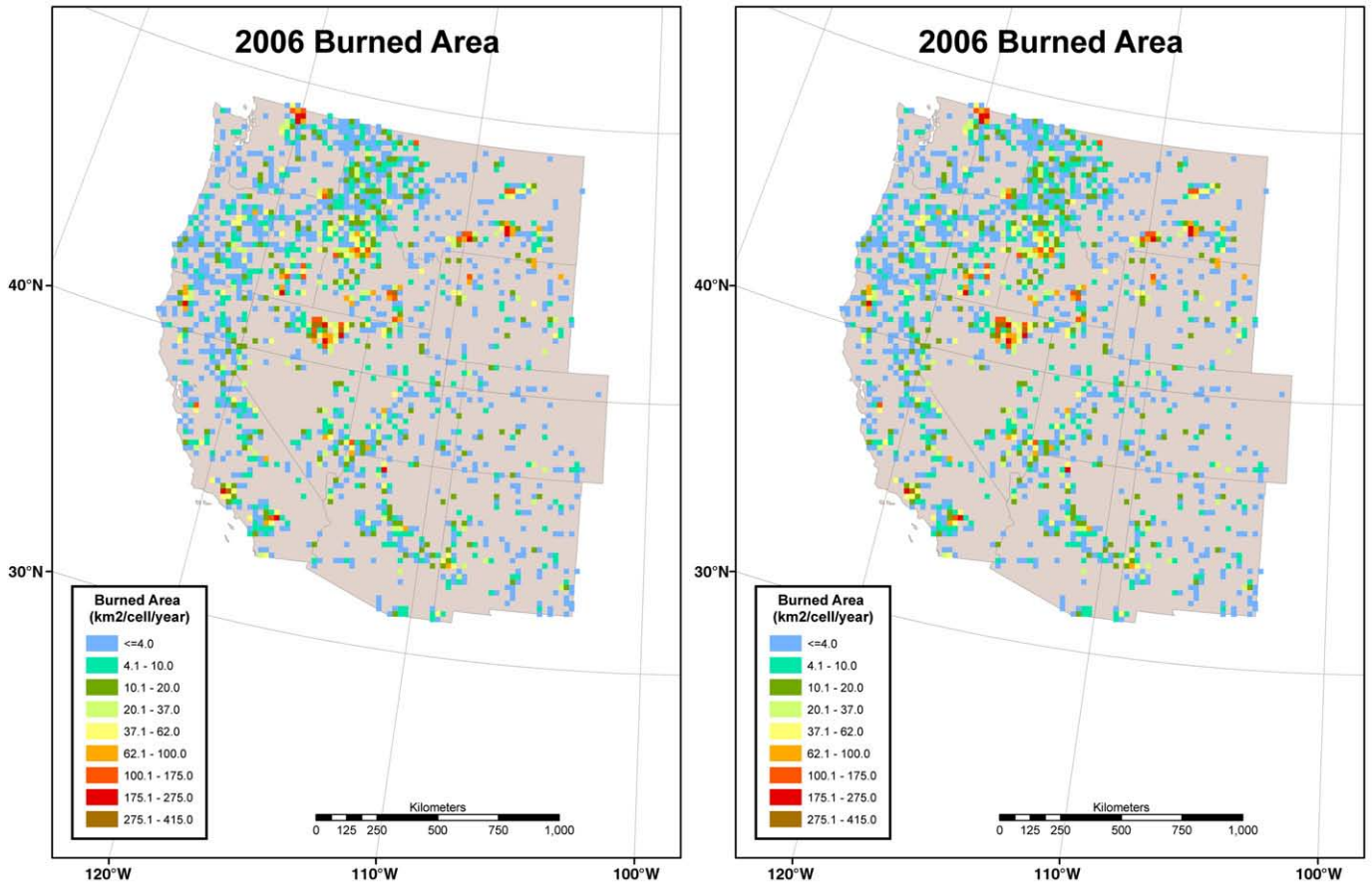

Fig. 9. Annual burned area measured with FiSL MODIS-DB burned area algorithm. Burned area aggregated as square km burned per 22-km × 22-km grid cell. The plotted data is the MODIS-DB burned area calibrated against the BARC reference dataset (Table 1).

number of fire events observed in that state during the month of concern. The parameters in Eq. (4) are the MR optimized results from Table 1 for calibration versus the BARC reference dataset. The Eq. (5) parameters are from the optimized empirical uncertainty function (Fig. 8).

$$BA_{(state,month)} = \sum_{i=1}^{nf} (a0 + a1 \times MOD_i) \quad (4)$$

$$RMSE_{(state,month)} = \sum_{i=1}^{nf} \left[b0 + b1 \times (MOD_i)^{b2} \right] \quad (5)$$

5. Discussion

5.1. Fire detection

The FiSL MODIS-DB burned area algorithm requires a MODIS active fire detection, based on the MXD14 algorithm, to initiate a fire event (Section 3.1.3). Therefore, the fire detection rate of our algorithm is, in fact, the MODIS active fire detection rate for the FiSL DB system. As expected, the MODIS active fire detection rate increases with fire size. Only 19% of all reference fires <1 km^2 are detected; while the detection rate is 87% for all fires >4 km^2 and 93% for all fires >10 km^2. While the majority of wildfires in the western U.S. are small, the large wildfires are responsible for most of the area burned and the fire emissions. Fires larger than 4 km^2 comprised 97% of the total area burned during 2003–2007, while fires with a final size exceeding 40 km^2 accounted for 78% of the total reported burned area (see Appendix A). For all but the largest fire size classes, the MODIS active fire algorithm is most effective at detecting forest fires (Fig. 5). With fires <10 km^2, the detection rate is markedly better for burning in forests compared with non-forest. We believe the difference in detection rates is related to differences in the fire behavior characteristics of the fuels, as discussed below. The difference between the forest and non-forest detection rates narrows with fire size, approaching parity for fires >20 km^2.

The MODIS-DB burned area algorithm was developed for large fire events (>4 km^2). A total of 53 reference fires larger than 4 km^2 were not detected by the FiSL MODIS-DB system. These 53 reference fires were also absent from the MODIS active fire detection dataset assembled by RSAC (URL: http://activefiremaps.fs.fed.us/gisdata.php). The missed large fires occurred predominantly in open shrublands and grasslands (51 of 53 fires, 94% of the total burned area; the remaining two fires occurred in savanna). The physical structure of grasses and shrubs, and their susceptibility to extreme drying, favors rapidly moving fires in these fuels (Anderson, 1982; Bradshaw et al., 1984; Rothermel, 1972). Additionally, grasslands and shrublands generally lack large diameter fuels or duff layers that burn and smolder behind the flaming front for extended periods (Anderson, 1982). These fire behavior characteristics suggest the MODIS active fire algorithm may have failed to detect these fires because they possessed rapidly moving flame fronts that were extinguished prior to the MODIS overpass and lacked postfrontal combustion. These wildfire characteristics of grass and shrub fuels may play a significant role in the lower overall detection rates for non-forest fires compared to forest fires (Fig. 5).

Recently, Hawbaker et al. (2008) (hereafter H08) investigated the detection rates of the MODIS active fire algorithm product in the U.S. using 361 reference fires (>=0.2 km^2) from 2003 to 2005. As in our

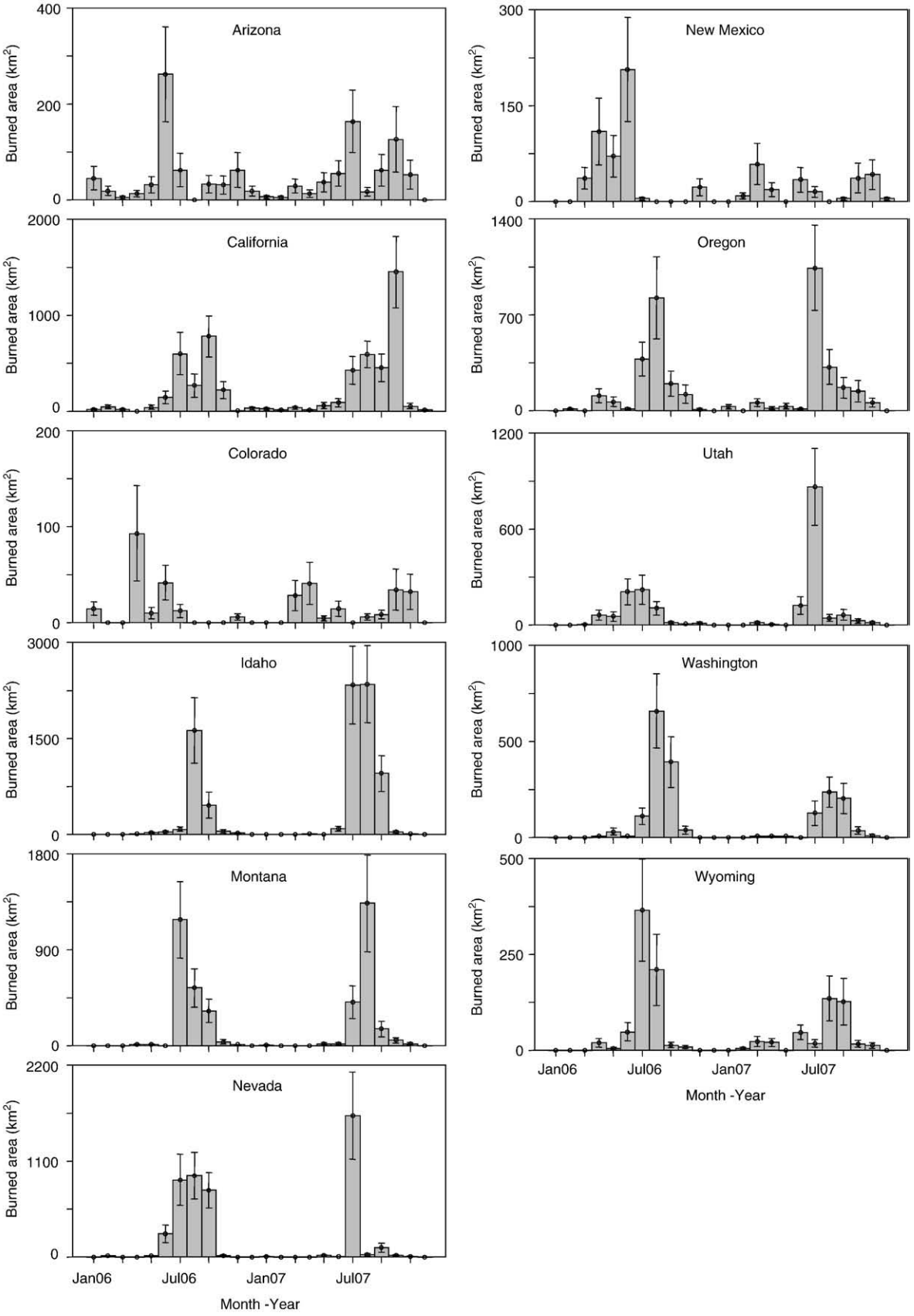

Fig. 10. Monthly, state level MODIS-based burned area and estimated uncertainty for 2006 and 2007. The burned area and uncertainties are based on MODIS-DB burned area calibrated against the BARC reference dataset (Table 1).

study, H08 found the MODIS active fire detection rate increased with fire size. They reported that 50% of all fires were detected at a size threshold of 1 km^2, and a ~90% detection rate for fires around 10 km^2 (Fig. 3 of H08). In order to compare our results with the findings of H08, we used logistic regression to estimate the proportion of reference fires detected by our MODIS-DB system as a function of fire size (see Appendix A). The FiSL MODIS-DB system detects 50% of the reference fires at size threshold of ~4 km^2 and has a detection rate of 67% at a fire size of 10 km^2. The significant difference in the detection rates between our study and H08 may by driven by two factors. First, the DB data from our single antenna receiving station provides fewer observations for the continental U.S. than the MODIS data set acquired from the NASA Land Processes Distributed Active Archive Center and used in H08. Secondly, it is possible the reference fire data sets used in the two studies have a significantly different distribution in fire type, i.e. the relative occurrence of forest and non-forest fires. Applying the logistic regression analysis to the subset of reference fires occurring in forest ($n=231$), we estimate the 50% detection threshold is ~0.4 km^2 and the probability of not detecting a 10 km^2 fire is negligible (Appendix A), results consistent with Fig. 5. H08 did not examine the role of land cover. Lacking detailed statistics describing the land cover of the reference fire data set used in H08, we cannot verify any impact of cover type in producing the different overall detection rates in the two studies.

The MODIS active fire algorithm is highly effective at detecting the large wildfires that dominate burned area and emissions in the western U.S. Performance of the MODIS active fire algorithm is exceptional in detecting large forest fires. Proficiency in detecting forest fires is crucial. While forested lands typically account for only ~25% of total burned area (Schwind, 2008), the heavy fuel loadings of western forests (Brown & Bevins, 1986; Brown & See, 1981) may lead to high emission intensities during the wildfire season. For this reason large forest fires are of particular concern to air quality forecasters and air shed managers.

5.2. Burned area measurement

5.2.1. Algorithm performance

The MODIS-DB burned area is highly correlated with the BARC burned area, but exhibits a large positive bias (Table 1). The bias may be related to the active fire detection buffering (circle area of 1 km^2) and/or burn scar edge effects. Comparison of our MODIS-DB active fire detection counts against the IP reference dataset yields a burned area to active fire detection ratio of 0.27 km^2 pixel^{-1} ($r=0.51$), indicating our 1 km^2 buffer is generous. The spectral tests of our burn scar algorithm are susceptible to false alarms. The algorithm filters for false alarms by testing for spatial and temporal proximity to active fire detections. A shortcoming of the spatial proximity filter is that false detections located outside the true fire perimeter, but within 5 km of a recent active fire detection, will pass the proximity tests and be confirmed a valid burn scar. The Shower Bath Complex Fire (Fig. 3) is one of the more egregious examples of failure in the spectral tests that evaded contextual filtering. False burn scar detections located outside the incident perimeter and not associated with any active fire detections contribute 116 km^2 to the burned area grid product (Fig. 3a and d). Of this 116 km^2, about 20 km^2 is attributable to areas burned by fire in 2005 and 2006. A significant swath of active fire detections and coincident burn scar detections were confirmed just outside the incident perimeter (this feature has been marked with an 'X' in Fig. 3). The detections in this area occurred in the days following acquisition of the final incident perimeter. It is likely the fire burned this region, totaling ~20 km^2, after the 'final' incident perimeter contained in the IP reference dataset was recorded. However, previous fires and burning that postdates the IP and BARC reference datasets explains only ~14% of the burned area differential for this fire event. The burned area grid product totals 611 km^2 for this fire event, more than double the area of the reference burn scar (286 km^2).

The algorithm appears sensitive to fire activity that is patchy or results in very low severity fire damage. The Chippy Fire triggered many active fire detections that were outside the validation burn scar (delineated with the BARC map), but within the incident fire perimeter (Fig. 2b). Many of these active fire detections are accompanied by burn scar detections (Fig. 2a). Only two burn scar detections fall outside the perimeter, and most of the active fire detections outside the perimeter are within ~1 km, the resolution of the active fire product. The coincidence of active fire and burn scar detections inside the fire perimeter, and lack of false detects beyond, suggests these regions experienced some degree of fire activity.

The burn scar algorithm successfully maps burned area from fire activity missed by the active fire detection product. In our evaluation we found it was not unusual for the active fire algorithm to miss substantial swaths of burned area that were properly mapped by the burn scar algorithm (Figs. 2–4). The absence of active fire detections in these areas may result from fire activity that occurred between MODIS observations or that produced thick smoke which obstructed detection. The propensity of the active fire product to miss significant burned area suggests algorithms that rely on active fire detections alone may have significant difficulty capturing the true spatial distribution of burned area.

5.2.2. Monthly burned area

The monthly large fire ($\geq$4 km^2) burned area by state, with estimated uncertainties, is presented in Fig. 10. In 2006 and 2007 the states of Idaho, California, Nevada, Montana, and Oregon accounted for ~75% of the total burned area in the western U.S. In the northern Rockies (Idaho, Montana, and Wyoming) and Nevada the burned area was concentrated in the middle to late summer (July–September), while burning in the Pacific Northwest peaked in the July and August and extended into October. The burned area is most broadly distributed throughout the year in Colorado, New Mexico, Arizona, and California. In most states, during most months, the absence of large fires resulted in a small total burned area, with a large measurement uncertainty that often approached $\pm$100%. However, when the burned area was dominated by large fire events the uncertainty in the monthly burned area was significantly better, ranging from $\pm$25% to $\pm$40% (e.g. July–September, 2007 in Idaho).

5.2.3. Annual burned area comparison with previous estimates

We now compare our annual burned area estimates with a previous remote sensing based estimate and NICC records. Zhang and Kondragunta (2008) (hereafter, ZK08) reported fire burned areas across the U.S. (2000–2006) derived from GOES Wildfire Automated Biomass Burning Algorithm (WF_ABBA). The results of ZK08 for 2006, interpolated from their Fig. 9, are given in Table 3 along with the burned area estimates of our study and NICC data. As previously discussed (Section 2.2), burned areas based on incident perimeters, like the NICC data, overestimate the true burned. On average 28% of the area inside the incident perimeters is unburned or burned with very low severity (Schwind, 2008). The NICC data presented in Table 3 have been adjusted by a factor of 0.72 to account for this overestimation. The purpose of this crude adjustment is to identify any gross differences in the state level burned area sums. The NICC statistics include prescribed fire, but not agricultural burning. ZK08 include prescribed and agricultural fire, while our burned area algorithm is designed to exclude observations in agricultural areas (Section 3.1.2). However, our estimates may include some contributions from agriculture fires due to limitations of the land cover/land use map used to mask agricultural lands.

5.2.3.1. FiSL vs. NICC. The FiSL state level estimates of burned area are well correlated with the NICC data ($r=0.95$, $p<0.0001$ for 2006 and 2007 combined; $r=0.88$, $p<0.001$ for 2006 only, 95% confidence interval, Pearson's correlation). In 2006, the FiSL burned area is markedly lower than the adjusted NICC data in New Mexico, Nevada, and Montana (-1440, -1005, and -877 km^2, respectively). The 2006

Table 3
Annual burned area estimates for the western US states in 2006.

State	Burned area (km^2)		
	MODIS-DB BAA	ZK08	NICC adjusted
Arizona	778 ± 429	1281	776
California	2465 ± 980	3128	2183
Colorado	265 ± 160	312	372
Idaho	2673 ± 1066	2250	2937
Montana	2352 ± 834	1331	3139
Nevada	2956 ± 912	1047	3851
New Mexico	579 ± 292	562	1958
Oregon	2066 ± 921	812	1875
Utah	807 ± 384	646	1042
Washington	1411 ± 493	1062	1261
Wyoming	742 ± 323	750	671

The calibrated MODIS-DB burned area estimate includes all observed fires>1 km^2. Uncertainties for the calibrated MODIS-DB burned area are ± RMSE predicted by Eq. (3a) using optimized parameters in Fig. 8. (b0 = 0.31, b1 = 0.57, b2 = 0.79). ZK08 burned area is interpolated from Fig. 9 of Zhang and Kondragunta (2008). The NICC burned area is the reported perimeter area (Section 2.2) reduced by a factor of 0.72 to account for the estimated unburned area inside the perimeter (Section 5.2.3).

fire activity in these states occurred largely in rangeland (see Appendix A). Even in Montana, roughly 70% of the burned area occurred in grasslands, shrublands, and croplands. We suspect the predominance of rangeland fire affected the difference in burned area for these three states due to the lower MODIS detection rate. The MODIS fire detection algorithm is less efficient for rangeland fires compared to forest fires (Section 4.2 and Fig. 5). Even large rangeland fires (>20 km^2) may completely evade MODIS detection (Section 5.1; also see H08).

5.2.3.2. FiSL vs. GOES WF_ABBA. The state level 2006 burned area estimates of our study are not well correlated with those of ZK08 ($r = 0.50$, $p = 0.11$, 95% confidence interval, Pearson's correlation). In general, the burned area results of ZK08 are significantly lower than the FiSL data (OLS regression: ZK08 = 540 + 0.42 * FiSL, $R^2 = 0.25$, units of km^2). Our burned area estimates exceed those of ZK08 substantially in Nevada, Oregon, and Montana in both in absolute (1909, 1254, 1021 km^2) and relative (182% 154%, 77%) terms. For all three states, the ZK08 estimated annual burned area falls outside the lower uncertainty bound estimated for the FiSL data; ZK08 provide no uncertainty estimate for the annual state sums of burned areas. With only one year of data, summed on an annual time scale, it is difficult to speculate on the factors driving the large differences in estimated burned area reported for Nevada, Oregon, and Montana. However, it is worth noting that a recent study of fire in the Brazilian Amazon found GOES WF_ABBA requires 4 times the active fire area needed by MXD14 to attain the same detection probability (Schroeder et al., 2008).

6. Conclusion

We have evaluated a MODIS-DB burned area mapping algorithm that combines active fire detections with single scene burn scar detection. The purpose of the algorithm is to provide burned area estimates for the development of wildfire emission inventories which may be used to forecast and evaluate the impact of wildfires on regional air quality. The FiSL MODIS-DB system is highly effective in detecting the large wildfires that dominate burned area and emissions in the western U.S. During 2006–2007 the system detected 100% of reference forest fires >2 km^2, 87% of all reference fires >4 km^2, and 93% of all reference fires >10 km^2. The burned area product is highly correlated with final incident fire perimeters and burned area derived from high resolution imagery. A Landsat based BARC burn scar reference dataset was used to calibrate the algorithm response and quantify the uncertainty in burned area. In studies employing remote sensing for the measurement of burned area, uncertainty is usually difficult to characterize in a useful manner and is often given only cursory attention. We employed an objective, empirical error based approach to quantify the uncertainty of our burned area measurement at the fire event level. Our description of uncertainty provides a metric that is meaningful in context of remotely sensed burned area and emission inventories. The uncertainty is ± 36% for fires 50 km^2 in size, improving to ± 31% at a fire size of 100 km^2. Fires in this size range account for a substantial portion of burned area in the western U.S. (77% of area is due to fires >50 km^2, and 66% results from fires >100 km^2). The dominance of large wildfires in burned area, duration, and emissions makes these events a significant concern of air quality forecasters and air shed regulators. The MODIS-DB algorithm maps these large fire events with an uncertainty that is small compared to the uncertainty of the other variables which also influence wildfire emissions (e.g. fuel loading, fuel consumption, and emission factors).

Burned area in the western U.S. is dominated by large fire events occurring during the summer and early fall. In 2006 and 2007, fires in Nevada and the northwest (Idaho, Montana, Oregon, Washington) accounted for ~72% of the total burned area, with most of the fire activity occurring during the months of July through September. Fire activity in California, which spanned June–October, comprised 16% of total burned area in the western U.S. The MODIS-DB algorithm measures monthly, state level burned area with uncertainty of ± 25% to ± 40% (relative to the BARC reference dataset) during the peak fire months.

Air quality forecasting and mitigation management require that wildfire emission estimates are available in a timely manner, with high temporal (hour to day) and spatial resolution (<4 km), to support real-time operations. With daily coverage at 1-km spatial resolution, and a quantified measurement uncertainty, the burned area product presented in this paper is well suited for the development of wildfire emission inventories. The algorithm's DB implementation enables time sensitive burned area mapping to support operational air quality forecasting.

Potential improvements to the MODIS-DB algorithm include modification to consider land cover type (or ecosystem) and adjustment of the active fire/burn scar buffering scheme. Implementing cover type specific temporal and spatial proximity tests for confirming burn scar detections and aggregating detections into fire events would likely reduce the uncertainty of the burned area product. Our findings indicate that the use of buffered burn scar detections alone may be a more accurate approach for the mapping of burned area. The inclusion of buffered (1-km^2) active fire detections in the construction of fire event buffers leads to an overestimate of burned area. A potential algorithm improvement would use active fire detections solely for the identification of valid burn scars through temporal and spatial proximity tests. Valid burn scar detections alone would be used to map burned area.

Acknowledgements

We would like to thank Jess Clark and his colleagues from the U.S. Forest Service, Remote Sensing and Application Center for providing the BARC data. We thank Alex Petkov and Holly Eissinger for assistance in preparation and analysis of the MODIS direct broadcast data. We also offer our thanks to four anonymous reviewers whose comments and suggestions improved this paper. This research was supported by U.S. Forest Service Research and Development, U.S. Forest Service National Fire Plan, and the NASA North American Carbon Program under Agreement NNH05AA86I. The views, opinions, and findings contained in these works are those of the authors and should not be interpreted as an official U.S. Forest Service or U.S. Government position, policy, or decision.

Appendix A

Fire occurrence

Fig. A1 depicts the cumulative fraction of burned area versus final fire size for 5043 fire events in the western U.S. from 2003–2007, as reported in Incident Management Situation Report (IMSR or 'SIT')

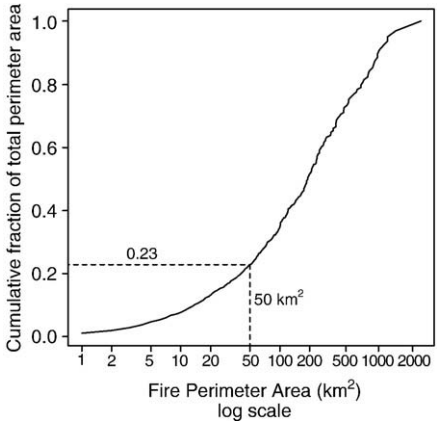

Fig. A1. Cumulative fraction of total wildfire burned area by fire size. *X*-axis is log scale. Figure includes all wildfires and wildland fire use fires in the western US from 2003–2007. The 'western US' is defined as the states of Arizona, California, Colorado, Idaho, Montana, Nevada, New Mexico, Oregon, Utah, Washington, and Wyoming.

database maintained by the National Interagency Fire Center (NIFC) in Boise, Idaho (URL: http://fam.nwcg.gov/fam-web/). While fire occurrence was dominated by small fires (58% of fires were less than 4 km^2) fires larger than 4 km^2 comprised 97% of the total burned area. Fires with a final size exceeding 40 km^2 accounted for 78% of the total reported burned area.

2006 Montana, Nevada, New Mexico

The cover type distribution of fire activity in Montana, Nevada, and New Mexico in 2006 was assessed using data from the 2006 Incident Management Situation Report (Section 2.2). The database includes fire point locations and fire perimeter areas. The dataset was imported into ESRI ARC Map and each fire location point was buffered with a circle of an area equal to the fire's final perimeter area. The buffered circles were intersected with the MOD12 land cover data product (Section 2.4), providing annual wildfire burned area by cover type at the state level. The fraction of total burned area attributed to grass, shrub, cropland, or barren land cover by state was: Montana 71%, Nevada 99%, and New Mexico 79%.

Fire detection

In order to make a direct comparison with Hawbaker et al. (2008), we followed their approach of relating the reference fire size to the proportion of fires not detected by the FiSL MODIS-DB system using logistic regression. We implemented logistic regression analysis with the logit link function using *R* statistical software (Everitt & Hothorn, 2006). The logit link function is used to transform the output of a linear regression fit into probabilities:

$$\text{Logit}(P) = A + Bx. \tag{A1}$$

The logistic function is the inverse of the logit function:

$$P = \frac{exp^{(A\,+\,Bx)}}{1 + exp^{(A\,+\,Bx)}}. \tag{A2}$$

In our analysis, P is the probability of the FiSL MODIS-DB station not detecting a reference fire of size x in hectares (100 hectare = 1 km^2). For comparison with Hawbaker et al. (2008), we used all reference fires ≥ 0.2 km^2. The results of our analysis are given in Table A1 and Fig. A2 (in Fig. A2 the reference fire size has been plotted in units of km^2 with a log scale for better display). The 50% detection rate threshold is 4.2 km^2 for all fires and 0.4 km^2 for forest fires alone. The result of the logistic regression analysis for the forest only data is less than robust ($p = 0.18$ for intercept); nevertheless, the result illustrates the higher detection rate for forest fires, a conclusion supported in the alternative analysis presented in Section 4.2.

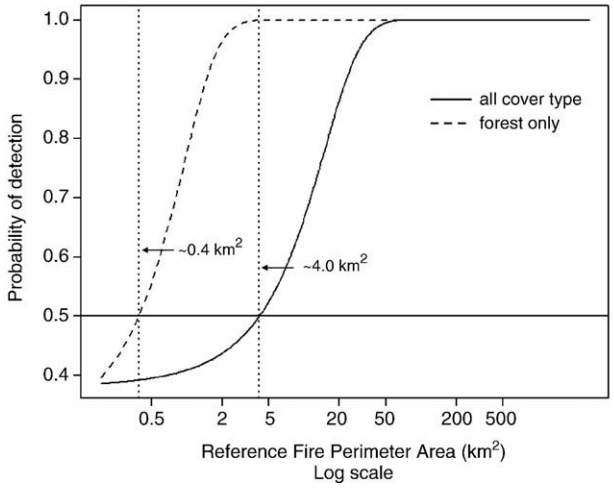

Fig. A2. Fire detection probability for the FiSL MODIS-DB system using the standard MOD14 algorithm. *X*-axis is log scale. The reference fire size has been plotted in units of km^2 (1 km^2 = 100 ha) with a log scale.

Table A1
Logistic regression parameters and fitting statistics for the fraction of reference fires not detected by the FiSLMODIS-DB system and the estimated 50% detection threshold.

Coefficient[a]	Estimate ± error[b]	*z*-value	*p*-value	*x* at *P* = 0.5[c]
All cover type (n = 831)				
A	0.4847 ± 0.1051	4.610	<0.001	4.2 km^2
B	−0.0012 ± 0.0001	−8.372	<0.001	
Forest only (n = 218)				
A	0.7990 ± 0.5994	1.333	<0.01	0.4 km^2
B	−0.0205 ± 0.0064	−3.195	0.18	

[a]Intercept (A) and slope (B) of Eqs. (A1) and (A2).
[b]Error is standard error.
[c]Estimated fire size at which 50% of fires are detected by the FiSL MODIS-DB system (Eq. (A2)).

References

Anderson, H. E. (1982). *Aids to determining fuel models for estimating fire behavior. Gen. Tech. Rep. INT-122* Ogden, UT: U.S. Department of Agriculture, Forest Service, Intermountain Forest and Range Experiment Station http://www.fs.fed.us/rm/pubs_int/int_gtr122.html

Bates, D. M., & Chambers, J. M. (1992). Nonlinear models. In J. M. Chambers & T. J. Hastie (Eds.), *Statistical Models in S* (pp. 421−453). Pacific Grove, California: Wadsworth and Brooks.

Bobbe, T., Finco, M. V., Quayle, B., Lannom, K., Sohlberg, R., & Parsons, A. (2003). Field measurements for the training and validation of burn severity maps from space borne remotely sensed imagery. *Joint Fire Science Program Final Project Report JFSP RFP 2001–2* Boise, ID: Joint Fire Science Program.

Bradshaw, L. S., Deeming, J. E., Burgan, R. E., & Cohen, J. D. (1984). The 1978 National Fire-Danger Rating System: Technical documentation. *General Technical Report INT-169* Ogden, UT: USDA Forest Service, Intermountain Research Station http://www.fs.fed.us/rm/pubs_int/int_gtr169.html

Brown, J. K, Bevins, C. D., (1986). Surface fuel loadings and predicted fire behavior for vegetation types in the northern Rocky Mountains. Research Note INT-358. U.S. Department of Agriculture, Forest Service, Intermountain Forest and Range Experiment Station, Ogden, UT.

Brown, J.K., & See, T.E. (1981). Downed dead woody fuel and biomass in the northern Rocky Mountains. General Technical Report INT-117, U.S. Department of Agriculture, Forest Service, Intermountain Forest and Range Experiment Station, Ogden, UT USA.

Brown, J. F., Loveland, T. R., Ohlen, D. O., & Zhu, Z. (1999). The global land-cover characteristics database: The users' perspective. *Photogrammetric Engineering and Remote Sensing, 65*, 1069−1074.

Chow, G. C. (1960). Test of equality between sets of coefficients in 2 linear regressions. *Econometrica, 28*, 591−605.

Clark, J., & Bobbe, T. (2004). Using remote sensing to map and monitor fire damage in forest ecosystems. In M. A. Wulder & S. E. Franklin (Eds.), *Understanding Forest Disturbance and Spatial Patterns: Remote Sensing and GIS Approaches* (pp. 246). London: Taylor & Francis.

Cocke, A. E., Fule, P. Z., & Crouse, J. E. (2005). Comparison of burn severity assessments using Differenced Normalized Burn Ratio and ground data. *International Journal of Wildland Fire*, *14*, 189−198.

DeBell, L. J., Talbot, R. W., Dibb, J. E., Munger, J. W., Fischer, E. V., & Frolking, S. E. (2004). A major regional air pollution event in the northeastern United States caused by extensive forest fires in Quebec, Canada. *Journal of Geophysical Research-Atmospheres*, *109*(D19) (Art. No. D19305).

Efron, B., & Tibshirani, R. (1993). *An introduction to the bootstrap* (pp. 105−121). New York: Chapman and Hall.

Epting, J., Verbyla, D., & Sorbel, B. (2005). Evaluation of remotely sensed indices for assessing burn severity in interior Alaska using Landsat TM and ETM+. *Remote Sensing of Environment*, *96*, 328−339.

Everitt, B. S., & Hothorn, T. (2006). *A handbook of statistical analyses using R* (pp. 92−93). London: Taylor & Francis, Inc.

Fraser, R. H., Li, Z., & Cihlar, J. (2000). Hotspot and NDVI differencing synergy (HANDS): A new technique for burned area mapping over boreal forest. *Remote Sensing of Environment*, *74*, 362−376.

Giglio, L., Descloitres, J., Justice, C. O., & Kaufman, Y. J. (2003). An enhanced contextual fire detection algorithm for MODIS. *Remote Sensing of Environment*, *87*, 273−282.

Giglio, L., van der Werf, G. R., Randerson, J. T., Collatz, G. J., & Kasibhatla, P. (2006). Global estimation of burned area using MODIS active fire observations. *Atmospheric Chemistry and Physics*, *6*, 957−974.

Glantz, S. A. (2002). *Primer of biostatistics* (pp. 230−288)., 5th edition New York: McGraw-Hill.

Global Land Cover Facility (2004). *Landsat Technical Guide, Global Land Cover Facility, Department of Geography* : University of Maryland Available at: http://glcf.umiacs.umd.edu/data/guide/technical/techguide_landsat.pdf

Hansen, M. C., DeFries, R. S., Townshend, J. R. G., & Sohlberg, R. (2000). Global land cover classification at the 1 km spatial resolution using a classification tree approach. *International Journal of Remote Sensing*, *21*, 1331−1364.

Hawbaker, T. J., Radeloff, V. C., Syphard, A. D., Zhu, Z. L., & Stewart, S. I. (2008). Detection rates of the MODIS active fire product in the United States. *Remote Sensing of Environment*, *112*, 2656−2664.

Ito, A., & Penner, J. E. (2004). Global estimates of biomass burning emissions based on satellite imagery for the year 2000. *Journal of Geophysical Research-Atmospheres*, *109*(D14) (Art. No. D14S05).

Key, C. H. (2006). Ecological and sampling constraints on defining landscape fire severity. *Fire Ecology*, *2*, 178−203.

Key, C. H., & Benson, N. C. (1999). Measuring and remote sensing of burn severity. In L. F. Neuenschwander, K. C. Ryan, & G. E. Goldberg (Eds.), *Proceedings of the Joint Fire Science Conference, Boise, Idaho 15–17 June, 1999*, *vol. II.* (pp. 284): University of Idaho and the International Association of Wildland Fire.

Key, C. H., & Benson, N. (2006). Landscape assessment: Sampling and analysis methods. *FIREMON: Fire effects monitoring and inventory system, Rep. RMRS-GTR-164-CD* (pp. LA1−LA55). Fort Collins, CO: U.S. Department of Agriculture, Forest Service, Rocky Mountain Research Station. http://www.fs.fed.us/rm/pubs/rmrs_gtr164.html

Koenker, R. W. (2005). *Quantile regression* (pp. 295−316). New York: Cambridge University Press.

Langmann, B., Duncan, B., Textor, C., Trentmann, J., & van der Werf, G. R. (2009). Vegetation fire emissions and their impact on air pollution and climate. *Atmospheric Environment*, *43*, 107−116.

Lapina, K., Honrath, R. E., Owen, R. C., Martin, M. V., & Pfister, G. (2006). Evidence of significant large-scale impacts of boreal fires on ozone levels in the midlatitude Northern Hemisphere free troposphere. *Geophysical Research Letters*, *33*(10) (Art. No. L10815).

Lentile, L. B., Holden, Z. A., Smith, A. M. S., Falkowski, M. J., Hudak, A. T., Morgan, P., et al. (2006). Remote sensing techniques to assess active fire characteristics and post-fire effects. *International Journal of Wildland Fire*, *15*, 319−345.

Li, R. R., Kaufman, Y. J., Hao, W. M., Salmon, J. M., & Gao, B. C. (2004). A technique for detecting burn scars using MODIS data. *Ieee Transactions on Geoscience and Remote Sensing*, *42*, 1300−1308.

Loboda, T., O'Neal, K. J., & Csiszar, I. (2007). Regionally adaptable dNBR-based algorithm for burned area mapping from MODIS data. *Remote Sensing of Environment*, *109*, 429−442.

Lohmann, U., & Feichter, J. (2005). Global indirect aerosol effects: A review. *Atmospheric Chemistry and Physics*, *5*, 715−737.

Michel, C., Liousse, C., Gregoire, J. M., Tansey, K., Carmichael, G. R., & Woo, J. H. (2005). Biomass burning emission inventory from burnt area data given by the SPOT-VEGETATION system in the frame of TRACE-P and ACE-Asia campaigns. *Journal of Geophysical Research-Atmospheres*, *110*(D9) (Art. No. D09304).

Mielke Jr., P. W., & Berry, K. J. (2001). *Permutation methods: a distance function approach* (pp. 352). New York: Springer-Verlag.

Miller, J. D., & Yool, S. R. (2002). Mapping forest post-fire canopy consumption in several overstory types using multi-temporal Landsat TM and ETM data. *Remote Sensing of Environment*, *82*, 481−496.

Morris, G. A., Hersey, S., Thompson, A. M., Pawson, S., Nielsen, J. E., Colarco, P. R., et al. (2006). Alaskan and Canadian forest fires exacerbate ozone pollution over Houston, Texas, on 19 and 20 July 2004. *Journal of Geophysical Research-Atmospheres*, *111* (D24) (Art. No. D24 S03).

Muhle, J., Lueker, T. J., Su, Y., Miller, B. R., Prather, K. A., & Weiss, R. F. (2007). Trace gas and particulate emissions from the 2003 southern California wildfires. *Journal of Geophysical Research-Atmospheres*, *112*(D3) (Art. No. D03307).

Naik, V., Mauzerall, D. L., Horowitz, L. W., Schwarzkopf, M. D., Ramaswamy, V., & Oppenheimer, M. (2007). On the sensitivity of radiative forcing from biomass burning aerosols and ozone to emission location. *Geophysical Research Letters*, *34*(3) (Art. No. L03818).

National Fire and Aviation Management (2008). *SIT report.*Boise, Idaho: National Interagency Fire Center Available from: http://fam.nwcg.gov/fam-web/

National Interagency Coordination Center (2008). *NICC statistics and summary*. Boise, Idaho: National Interagency Fire Center Available from: http://www.nifc.gov/nicc/predictive/intelligence/intelligence.htm

Phuleria, H. C., Fine, P. M., Zhu, Y. F., & Sioutas, C. (2005). Air quality impacts of the October 2003 Southern California wildfires. *Journal of Geophysical Research-Atmospheres*, *110* (D7) (Art. No. D07 S20).

Pu, R., Li, Z., Gong, P., Csiszar, I., Fraser, R., Hao, W. M., et al. (2007). Development and analysis of a 12-year daily 1-km forest fire dataset across North America from NOAA/AVHRR data. *Remote Sensing of Environment*, *108*, 198−208.

Rothermel, R. C. (1972). *A mathematical model for predicting fire spread in wildland fuels. INT-115* Ogden, UT: U.S. Department of Agriculture, Forest Service, Intermountain Forest and Range Experiment Station.

Roy, D. P., Boschetti, L., Justice, C. O., & Ju, J. (2008). The collection 5 MODIS burned area product — Global evaluation by comparison with the MODIS active fire product. *Remote Sensing of Environment*, *112*, 3690−3707.

Safford, H. D., Miller, J., Schmidt, D., Roatrh, B., & Parsons, A. (2008). BAER soil burn severity maps do not measure fire effects to vegetation: A comment on Odion and Hanson (2006). *Ecosystems*, *11*, 1−11.

Sapkota, A., Symons, J. M., Kleissl, J., Wang, L., Parlange, M. B., Ondov, J., et al. (2005). Impact of the 2002 Canadian forest fires on particulate matter air quality in Baltimore City. *Environmental Science & Technology*, *39*, 24−32.

Schwind, B. (2008). Monitoring trends in burn severity: Report on the PNW & PSW fires — 1984 to 2005. *USDA Forest Service, Remote Sensing Applications Center (RSAC); US Geological Survey, Center for Earth Resources Observations and Science (EROS)*. Available online: http://mtbs.gov/(compiler).

Schroeder, W., Prins, E., Giglio, L., Csiszar, I., Schmidt, C., Morisette, J., et al. (2008). Validation of GOES and MODIS active fire detection products using ASTER and ETM+ data. *Remote Sensing of Environment*, *112*, 2711−2726.

Seiler, W., & Crutzen, P. J. (1980). Estimates of gross and net fluxes of carbon between the biosphere and the atmosphere from biomass burning. *Climate Change*, *2*, 207−247.

Simon, M., Plummer, S., Fierens, F., Hoelzemann, J. J., & Arino, O. (2004). Burnt area detection at global scale using ATSR-2: The GLOBSCAR products and their qualification. *Journal of Geophysical Research-Atmospheres*, *109*(D14) (Art. No. D14 S02).

Simpson, I. J., Rowland, F. S., Meinardi, S., & Blake, D. R. (2006). Influence of biomass burning during recent fluctuations in the slow growth of global tropospheric methane. *Geophysical Research Letters*, *33*(22) (Art. No. L22808).

Spracklen, D. V., Logan, J. A., Mickley, L. J., Park, R. J., Yevich, R., Westerling, A. L., et al. (2007). Wildfires drive interannual variability of organic carbon aerosol in the western US in summer. *Geophysical Research Letters*, *34*(16) (Art. No. L16816).

Tansey, K., Gregoire, J. M., Binaghi, E., Boschetti, L., Brivio, P. A., Ershov, D., et al. (2004). A global inventory of burned areas at 1 km resolution for the year 2000 derived from SPOT VEGETATION data. *Climatic Change*, *67*, 345−377.

Turner, D. L. (2006). *MRPP: an alternative approach.* Available from: http://fsweb.rmrs.fs.fed.us/statistics/statmethods/IntroMRPP.html

van der Werf, G. R., Randerson, J. T., Giglio, L., Collatz, G. J., Kasibhatla, P. S., & Arellano, A. F. (2006). Interannual variability in global biomass burning emissions from 1997 to 2004. *Atmospheric Chemistry and Physics*, *6*, 3423−3441.

van Wagtendonk, J. W., Root, R. R., & Key, C. H. (2004). Comparison of AVIRIS and Landsat ETM+ detection capabilities for burn severity. *Remote Sensing of Environment*, *92*, 397−408.

Vermote, E. F., El Saleous, N. Z., & Justice, C. O. (2002). Atmospheric correction of MODIS data in the visible to middle infrared: First results. *Remote Sensing of Environment*, *83*, 97−111.

Wiedinmyer, C., Quayle, B., Geron, C., Belote, A., McKenzie, D., Zhang, X. Y., et al. (2006). Estimating emissions from fires in North America for air quality modeling. *Atmospheric Environment*, *40*, 3419−3432.

Wilcox, R. R. (2005). *Introduction to robust estimation and hypothesis testing* (pp. 413−464). Burlington, MA: Elsevier Academic Press.

Zhang, X. Y., & Kondragunta, S. (2008). Temporal and spatial variability in biomass burned areas across the USA derived from the GOES fire product. *Remote Sensing of Environment*, *112*, 2886−2897.